International Journal of
Turbomachinery
Propulsion and Power

MDPI

Review

Experimental Investigation Techniques for Non-Ideal Compressible Fluid Dynamics

Stefan aus der Wiesche

Department of Mechanical Engineering, Muenster University of Applied Sciences, 48565 Steinfurt, Germany; wiesche@fh-muenster.de; Tel.: +49-2551-9-62272

Abstract: The rising number of applications of the organic Rankine cycle (ORC) or supercritical CO_2 (sCO_2) power systems have shaped a new branch of fluid mechanics called non-ideal compressible fluid dynamics (NICFD). This field of fluid mechanics is concerned with flows of vapors or gases, which are characterized by substantial deviations from the perfect gas model. In extreme cases, even non-classical gas dynamic phenomena could occur. Although these non-ideal compressible flows are the subject of sophisticated numerical simulation studies today, there is also a growing need for experimental data for validating purposes. In the last couple of years, new experimental test rigs designed for investigating non-ideal compressible fluid dynamics have been developed and commissioned. Classical practical measurement techniques are currently being re-developed and applied to non-ideal compressible flows. Despite its substantial relevance, information about these measurement techniques and their differences from conventional methods in the open literature is scarce. The present review article is an attempt to reduce that gap. After briefly discussing the thermodynamics and fluid dynamics of non-ideal compressible flows, the currently available test rigs and their utilized measurement techniques are reviewed. This review discusses schlieren optical investigations, pneumatic and laser-optical methods, and hot-wire anemometry for non-ideal compressible flows.

Keywords: compressible flow; non-ideal gas; ORC; flow measurement; test rigs; pitot probes; schlieren systems; LDV; PIV; hot-wire anemometry

Citation: Wiesche, S.a.d. Experimental Investigation Techniques for Non-Ideal Compressible Fluid Dynamics. *Int. J. Turbomach. Propuls. Power* **2023**, *8*, 11. https://doi.org/10.3390/ijtpp8020011

Academic Editors: Rodolfo Bontempo and Tony Arts

Received: 15 December 2022
Revised: 21 February 2023
Accepted: 23 February 2023
Published: 3 April 2023

1. Introduction

Organic Rankine cycle (ORC)-based power systems are being extensively investigated for heat-to-electric power conversion from solar and geothermal heat sources and waste heat recovery. The ORC technology offers a high potential [1] for meeting environmental requirements and reducing climate issues. The rising number of applications of organic Rankine cycle (ORC) power systems [1,2] has increased the relevance of a new branch of fluid mechanics called non-ideal compressible fluid dynamics (NICFD). In recent years, the interest in supercritical CO_2 (sCO_2) power systems has led to a further need to better understand the gas dynamics of fluids that are far away from the usual perfect gas behavior [3]. NICFD are concerned with flows of vapors or gases that are characterized by substantial deviations from the perfect gas model. In extreme cases, theoretical analyses [4–6] even predict the occurrence of non-classical gas dynamical phenomena, including the formation and propagation of expansion or rarefactive shocks, sonic shocks, double sonic shocks, and shock splitting.

In thermodynamics, a perfect gas is a unique gas model that differs from real gases in specific ways that make calculations easier to handle. In all perfect gas models, intermolecular forces are neglected. All perfect gas models are ideal gas models in the sense that they all follow the ideal gas equation of state

$$p = \rho RT, \tag{1}$$

with p signifying pressure, ρ signifying density, T signifying temperature, and R signifying the specific gas constant. However, the term perfect gas model is often invoked as a combination of the ideal gas equation of state (1) with specific additional assumptions regarding the variation in the heat capacity with temperature [7]. The branch of fluid mechanics that deals with the compressible flow of fluids violating the ideal gas equation of state (1) are called non-ideal compressible fluid dynamics (NICFD); see, for instance, [8]. This review paper is primarily concerned with experimental techniques applied in this field.

In principle, it is always possible to formulate an equation of state

$$p = \rho ZRT \tag{2}$$

for arbitrary fluids by introducing an additional compressibility factor Z, which is generally a function of two independent thermodynamic variables: pressure p, and temperature T, or specific entropy s. For a perfect gas, the identity $Z = 1$ holds. However, $Z \neq 1$ is a necessary condition, but not a sufficient one, for fluids to exhibit non-ideal compressible flow behavior. Section 2 will explain the different kinds of gas dynamics in more detail. For the present purpose, it is sufficient to notice that non-ideal compressible flow phenomena outside the well-known perfect gas aerodynamics frequently characterize real gases or vapors.

The interest in studying non-ideal compressible fluid dynamics (NICFD) can be traced back to early theoretical works by Duhem [9], Becker [10], Bethe [11], and Zel'dovich [12]. Later, Thompson provided a foundational article in 1971 [13] about the gas dynamics of fluids whose properties do not comply with the ideal gas law (1). This research was driven by the fundamental academic question regarding the possibility of fluids for which non-classical or inverted gas dynamics might occur. This exciting question is still open, and a final answer cannot be given so far. Independently and with a different goal, aerodynamicists began in the 1990s to re-consider non-ideal compressible flow effects in wind tunnel testing [14–16]. Their objective was to achieve a higher Reynolds numbers in wind tunnel testing using heavy gases consisting of complex molecules. It was shown that the transonic similarity theory only partially successfully transformed the heavy gas results into equivalent nitrogen or air results. Aircraft designers demanded the latter. Due to the non-ideal gas dynamics, it was impossible to obtain reliable correction schemes for predicting shockwave boundary layer interactions for similar perfect gas flows based on the non-ideal compressible flow measurements. Consequently, the interest of aircraft designers in the aerodynamics of non-ideal gases diminished. Anders et al. [16] explained the failure of the transonic similarity theory regarding the shock/boundary layer interaction by the fact that the transonic similarity theory one bases on small disturbance potential flow theory. Thus, an inviscid transformation will not account for the difference in boundary layers for two different gases.

NICFD are essential for understanding phenomena occurring in industrial processes working with organic vapors or heavy gases [17] at higher speed levels. Turbomachinery operating partly in the NICFD regime is expected in the oil and gas industry [18]. NICFD effects occur in the organic Rankine cycle (ORC) [2] and in supercritical carbon dioxide (sCO2) [19] power systems. The number of numerical studies dealing with NICFD effects is numerous, but dedicated descriptions of corresponding test facilities and experimental works are relatively scarce [20]. However, there is a solid need to validate sophisticated computational fluid dynamics (CFD) models and schemes. During the last few years, progress has been made regarding experimental techniques and their applications to NICFD research. The technical challenges associated with designing and operating test facilities for NICFD research are arguably higher than conventional wind tunnels or test rigs for air. Due to the elevated pressure and temperature levels usually required for studying

NICFD effects, standard flow measurement techniques require substantial design and data reduction modifications.

This paper reviews the available experimental investigation techniques for non-ideal compressible fluid dynamics. Since the author of this paper is working in the field of ORC power systems, this review focuses on experimental methods that have been used and considered in the ORC research community. This contribution focuses on measurement techniques for testing organic vapor flows in ORC power system turbomachinery.

2. Non-Ideal Compressible Fluid Dynamics

Before starting with a review of experimental test facilities and measurement techniques, it is necessary to review some fundamentals of non-ideal compressible fluid dynamics. The need to investigate non-ideal compressible fluid dynamics and their differences with reference to conventional testing for steam and gas turbines requires sound knowledge of the fundamental thermodynamic and fluid mechanics relations. In this context, it is helpful to distinguish between thermodynamically non-ideal gas behavior and non-ideal fluid mechanical phenomena that are relevant to turbomachinery applications.

2.1. Thermodynamical Classification of Gas Dynamics

In 1942, Landau introduced a non-dimensional parameter

$$\frac{v^3}{a^2}\left(\frac{\partial^2 p}{\partial v^2}\right)_s$$

for the evaluation of the curvature of isentropes in the p,v diagram [21]. The curvature of the isentropes is of considerable interest, because a negative curvature is required for rarefaction shocks [4]. In classical gas dynamics, only compression shocks can exist due to the second law of thermodynamics. The possibility that only compression shocks can be observed is directly related to a positive curvature of the isentropes of the involved gases. Later, Hayes [22] denoted Landau's parameter with the symbol Γ and introduced a multiplier ½. Following Thompson [13], it is common to call

$$\Gamma = \frac{1}{2}\frac{v^3}{a^2}\left(\frac{\partial^2 p}{\partial v^2}\right)_s = 1 + \frac{\rho}{a}\left(\frac{\partial a}{\partial \rho}\right)_s \tag{3}$$

the "fundamental derivative of gas dynamics." In Equation (3), a denotes the speed of sound, and v is the specific volume ($v = 1/\rho$). Using general thermodynamic relations, further different expressions for the fundamental derivative of gas dynamics Γ can be obtained [13]. In the case of a perfect gas, by obeying Equation (1), the fundamental derivative Γ reduces to the simple relation

$$\Gamma = \frac{1}{2}(\gamma + 1) \tag{4}$$

with $\gamma = c_p/c_v$ signifying the isentropic exponent of the perfect gas. Since $c_p > c_v$ holds for a perfect gas, the fundamental derivative Γ is larger than the one for a perfect gas. This is valid in classical compressible fluid dynamics with an increasing speed of sound and with pressure at a constant entropy. Classical non-ideal compressible fluid dynamics occur for $0 < \Gamma < 1$. Then, the speed of sound decreases with increasing pressure at a constant entropy. A fluid with that property is called a "dense gas" or "dense vapor." In the particular, yet academic case where $\Gamma = 1$, the speed of sound is a constant. Dense gases exist in nature, and Figure 1 illustrates an isentropic expansion process starting in the dense vapor regime for MDM. Below the contour line $\Gamma = 1$, MDM behaves like an ideal gas. This is referred to as a dilute gas regime. However, the region with $\Gamma < 1$ is not tiny in the T,s diagram of MDM, and non-ideal compressible fluid dynamics must be considered for typical turbine expansion processes [23].

The question of whether fluids with $\Gamma < 0$ exist is still open [24]. It is likely that the study of the fluid dynamics of fluids obeying $\Gamma < 0$ will be more of an academic issue than

a practical engineering task. Thermodynamics laws permit such a dense vapor in principle, but so far, no actual working fluid has been found that fulfills the condition $\Gamma < 0$. For ORC applications, the range $0 < \Gamma < 1$ is relevant. Still, in a substance with $\Gamma < 0$, non-classical non-ideal compressible fluids dynamics, such as rarefaction shocks or compression fans, would occur. Non-classical gas dynamics can be interpreted as an inversion of classical gas dynamics. Such non-classical fluids are also called BZT fluids in honor of the contributions from Bethe, Zel'dovich, and Thompson after a suggestion by Cramer (see [4], especially pages 91–145). The condition $\Gamma < 0$ corresponds to a speed of sound decreasing with pressure at a constant entropy.

Table 1 lists the classification of gas dynamics from the thermodynamic point of view. In supersonic turbines working with a BZT fluid, more lower shock losses could occur than for those working with classical fluids. This interesting prediction was first made in a numerical study [25] considering the aerodynamic testing of airfoils in heavy gases.

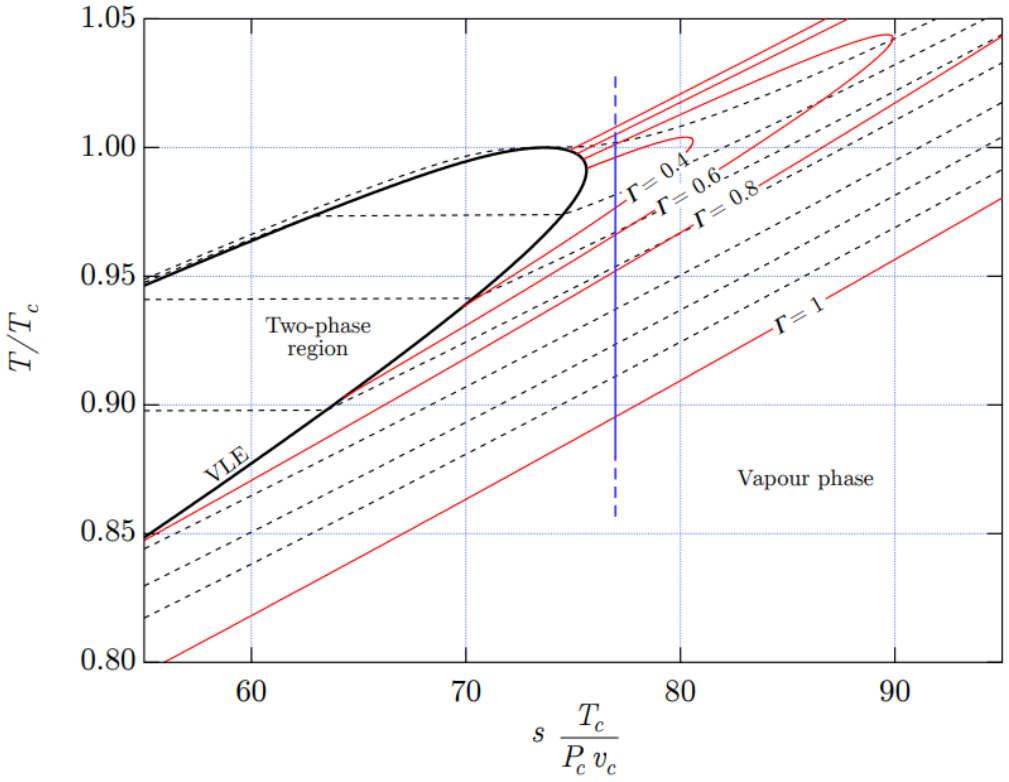

Figure 1. Normalized T,s diagram for MDM (from [23]), computed from the reference equation of state [26]. The red lines correspond to states with a constant Γ. The black dotted lines illustrate the behavior of the isobars. A potential isentropic expansion process is shown as a blue line (see typical expansion processes in some test rigs described in Section 3).

Table 1. Classification of gas dynamics from a thermodynamic point of view (following a scheme proposed by Thompson [13]).

Γ	**Fluid**	**Sound Speed Variation**	**Classification of Gas Dynamics**
$\Gamma > 1$	Perfect gas	$(\partial a/\partial p)_s > 0$	classical
$\Gamma = 1$		$(\partial a/\partial p)_s = 0$	classical non-ideal
$\Gamma < 1$	Dense gas	$(\partial a/\partial p)_s < 0$	classical non-ideal
$\Gamma = 0$		$(\partial a/\partial p)_s < 0$	non-classical non-ideal
$\Gamma < 0$	BZT fluids	$(\partial a/\partial p)_s < 0$	non-classical non-ideal

2.2. Classification for Turbomachinery Flows

An alternative classification of compressible flows results from the viewpoint of turbomachinery and their aerodynamical testing. Here, a hierarchy of fluids can be derived based on a formal analysis of the governing equations of compressible flows as introduced by Traupel [27,28]. Since these essential works are, somewhat surprisingly, not available in English, a more detailed discussion might be valuable for several readers.

The bases of turbomachinery flows are the continuity equation, the Navier–Stokes equation, and the energy equation:

$$\frac{\partial \rho}{\partial t} + \nabla(\rho \mathbf{w}) = 0 \tag{5}$$

$$\frac{\partial \mathbf{w}}{\partial t} + (\mathbf{w} \cdot \nabla)\mathbf{w} = \mathbf{f} - \frac{1}{\rho}(\nabla p + \mathbf{S}) \tag{6}$$

$$\left(\frac{\partial}{\partial t} + (\mathbf{w} \cdot \nabla)\right)\left(h + \frac{1}{2}\mathbf{w}^2\right) = (\mathbf{w} \cdot \mathbf{f}) + \frac{1}{\rho}\left((\mathbf{w} \cdot \mathbf{S}) + \mu\mathbf{\Phi} + \nabla(\lambda \nabla T)\right) \tag{7}$$

Here, **w** is the velocity vector, **f** is the body force vector, **S** is the stress tensor (a function of velocity and viscosity), and **Φ** represents the viscous dissipation. The thermodynamic variables are the density ρ, the pressure p, the temperature T, and the specific enthalpy h. The transport coefficients are the dynamic viscosity μ and the thermal conductivity λ.

Within a certain temperature range, the specific enthalpy h of a perfect gas obeys a simple relation using the specific heat at constant pressure c_p. By inserting

$$\rho = \frac{p}{RT} \qquad \text{and} \quad h = c_p T \tag{8}$$

into the general governing Equations (5)–(7), the perfect gas flow governing equations become

$$\frac{\partial}{\partial t}\left(\frac{p}{T}\right) + \nabla\left(\frac{p}{T}\boldsymbol{w}\right) = 0 \tag{9}$$

$$\frac{\partial \mathbf{w}}{\partial t} + (\mathbf{w} \cdot \nabla)\mathbf{w} = \mathbf{f} - \frac{RT}{p}(\nabla p + \mathbf{S}) \tag{10}$$

$$\left(\frac{\partial}{\partial t} + (\mathbf{w} \cdot \nabla)\right)\left(c_p T + \frac{1}{2}\mathbf{w}^2\right) = (\mathbf{w} \cdot \mathbf{f}) + \frac{RT}{p}\left((\mathbf{w} \cdot \mathbf{S}) + \mu\mathbf{\Phi} + \nabla(\lambda \nabla T)\right) \tag{11}$$

This set of equations governs turbomachinery working with perfect gases. A relatively similar formal structure as the set of Equations (9)–(10) can be derived for a gas obeying the equation of state

$$h = \frac{\gamma}{\gamma - 1}\frac{p}{\rho} = \frac{\gamma}{\gamma - 1}ZRT \tag{12}$$

This equation of state is more general than the ideal gas model described by Equation (8). Inserting Equation (12) into the set of Equations (5)–(7) yields

$$\frac{\partial}{\partial t}\left(\frac{p}{h}\right) + \nabla\left(\frac{p}{h}\boldsymbol{w}\right) = 0 \tag{13}$$

$$\frac{\partial \boldsymbol{w}}{\partial t} + (\boldsymbol{w} \cdot \nabla)\boldsymbol{w} = \boldsymbol{f} - \frac{\gamma - 1}{\gamma}\frac{h}{p}(\nabla p + \boldsymbol{S}) \tag{14}$$

$$\left(\frac{\partial}{\partial t} + (\boldsymbol{w} \cdot \nabla)\right)\left(h + \frac{1}{2}\boldsymbol{w}^2\right) = (\boldsymbol{w} \cdot \boldsymbol{f}) + \frac{\gamma - 1}{\gamma}\frac{h}{p}\left((\boldsymbol{w} \cdot \boldsymbol{S}) + \mu\boldsymbol{\Phi} + \nabla(\lambda \nabla T)\right) \tag{15}$$

The above set of Equations (13)–(15) has the same formal structure as the set (9)–(11) if the temperature T in the perfect gas Equations (9)–(11) is replaced with the expression $((\gamma - 1)/\gamma)h/R$ and if c_p is replaced with $\gamma R/(\gamma - 1)$. The only exception is the last heat conduction term ($\nabla(\lambda \nabla T)$) in Equation (15). This means that heat conduction phenomena are formally excluded from that similarity. However, heat conduction effects are typically only of minor importance for several turbomachinery applications.

The main conclusion of the above analysis is that gases defined by Equation (8) or Equation (12) are essentially equivalent for turbomachinery flow analysis purposes. Equation (12) ensures that a fluid behaves like a quasi-perfect gas. For such a fluid, conventional testing applies, and no significant non-ideal gas dynamics would be expected in turbomachinery flows. Traupel [27] showed that Equation (12) could only be fulfilled for gases for which (i) the compressibility factor Z is a unique function of the entropy s as a single variable (i.e., $Z = f(s)$), and for which (ii) a constant isentropic exponent exists for pressure–volume relations (i.e., pv^{γ} = constant). For non-perfect gases, the nomenclature γ_{pv} is also in use for the isentropic exponent for pressure–volume relations to distinguish it from the ratio of the specific heats $\gamma = c_p/c_v$ [29]. A fluid obeying Equation (12) is called a "perfect vapor" [28]. Steam is an example of a perfect vapor for a broad range of thermodynamic conditions. This thermodynamic fact explains why steam turbine designers can use data from conventional wind tunnels working with air.

For non-perfect gases violating Equation (12), a different formal structure of the governing equations follows. Hence, from the viewpoint of turbomachinery flows and corresponding testing, the classification listed in Table 2 is relevant. The category of Table 2 is also essential for dimensional analysis [30]. Whereas gas turbines, and, to a large extent, steam turbine flows, can be aerodynamically tested using conventional wind tunnels and measurement equipment, organic vapor testing requires, in general, special efforts. Furthermore, correction schemes might not apply for relating results obtained for a perfect gas to the dense gas regime of an organic vapor. It should be noted that an organic vapor might behave like a perfect gas if the processes take place in the range where the compressibility factor $Z \approx 1$ (see Figure 1). However, in the thermodynamic range where Z differs significantly from unity, non-ideal compressible flow phenomena are likely to occur. From a rigorous theoretical point of view, the derivatives of Z,

$$\left(\frac{\partial Z}{\partial p}\right)_s \text{ and } \left(\frac{\partial Z}{\partial T}\right)_s ,$$

and not the absolute values of Z are relevant, because non-vanishing derivates of Z for s = *constant* reflect the condition $Z \neq f(s)$. This fundamental fact is somewhat obscured, because many authors only look to the absolute value of the compressibility factor Z. They do not consider the impact of thermodynamic variables on Z in detail. However, most fluids are characterized by the fact that thermodynamic regions where $Z < 1$ hold are also regions where $Z \neq f(s)$.

Table 2. Classification of fluid mechanics (following Traupel [27,28]).

Z	Fluid	Example	Aerodynamic Testing
$Z = 1$	Perfect gas	Air	conventional wind tunnel testing
$Z = f(s)$	Perfect vapor	Steam	mainly conventional (correction schemes applicable)
$Z \neq f(s)$	Non-ideal gas	Organic vapors	correction schemes might not apply

2.3. Similitude and Experiments with Model Configurations

The dimensional analysis and the concept of similitude are highly relevant for planning experiments [31]. In the case of steam and gas turbines, Dejc and Trojanovskij [32] summarized, in the outcome of dimensional analysis, that five fundamental similarity numbers (or similarity criteria) must be considered for turbomachinery testing: the

isotropic exponent γ, the Prandtl number *Pr*, the Reynolds number *Re*, the Mach number *Ma*, and the flow coefficient ϕ. These five fundamental similarity numbers are a direct consequence of the validity of the fundamental Equations (9)–(11) or (13)–(15) as discussed in [30]. Furthermore, in experiments, the same roughness and turbulence level as that which occurs in the original turbomachine should be provided.

In the case of a working fluid violating the equation of state (1) or (12), as in the case of organic vapor, the above five similarity numbers no longer establish a complete set from the viewpoint of dimensional analysis. At least one other similarity number describing the non-ideality of the fluid must be considered [30]. In actual testing, it is often necessary to use the same working fluid in laboratory experiments as what is used in the original engine, because it is practically impossible to find other testing fluids exhibiting the same thermodynamic behavior as the working fluid under original conditions. Hence, conducting experiments dealing with NICFD requires test rigs that precisely use the same working fluids as those used in the original turbomachines or power systems. That represents a significant difference from the single-phase-flow aerodynamical testing of steam and gas turbines, which can be performed in conventional wind tunnels with air as a working fluid.

3. Test Facilities

Only aerodynamic testing related to turbomachinery applications will be considered in the following. Test rigs for entire ORC power systems (see, for instance, [33–35]) are hence excluded from this review. Also excluded are conventional test rigs for heat exchangers working with vapors. A brief overview of currently used test rigs for non-ideal compressible flow investigations was recently published [36]. A good review, also including the history of test facilities, is provided in [20].

3.1. Classification

The facilities for aerodynamic testing of non-ideal compressible flow dynamics can be classified into intermittently and continuously working systems (see Figure 2). The use of a "wind tunnel" for test facilities working with organic vapors might be somewhat misleading (the expression "vapor tunnel" would be clearer), but it is the usual terminology in aerodynamics [14–16].

The advantage of intermittently working fluids is their relatively low power consumption (but at the cost of a substantial charging time for each test run). Significant power is required to drive a continuously working wind tunnel for non-ideal fluids, because their density is high. Although their speed of sound is relatively low (of the order a = 100 m/s), even a moderate volume flow rate leads to high mass flow rates and, hence, to high power consumptions. On the other hand, a continuously running wind tunnel has the advantage that long-time measurements or even steady-state operation are possible, whereas intermittently working test facilities require fast measurement techniques.

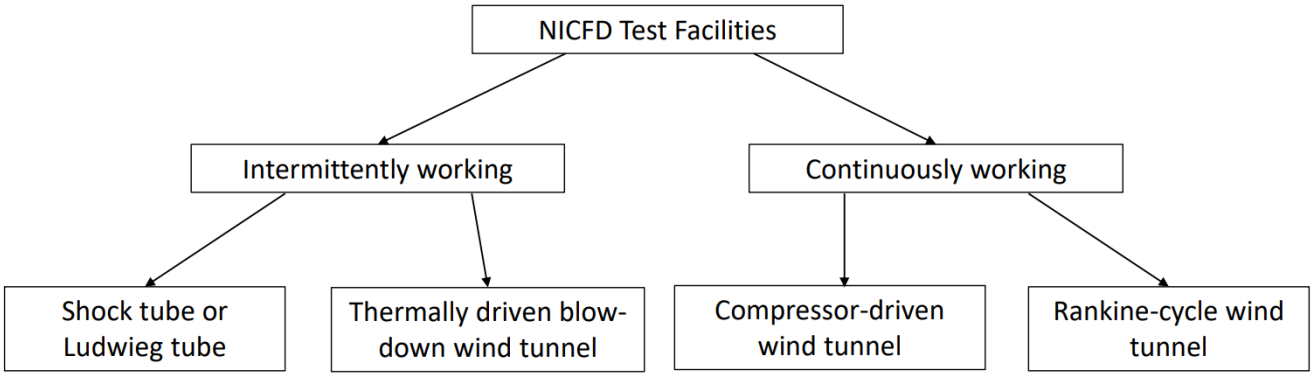

Figure 2. Classification of test rigs for non-ideal compressible fluid dynamics.

3.2. Shock Tubes or Ludwieg Tubes

A shock tube is a device for investigating high Mach number flows. It consists of a tube with a rectangular or circular cross-section, in which a gas at low pressure and a gas at high pressure are separated using some form of a diaphragm. Details can be found in the classical texts [37–39]. The diaphragm bursts under predetermined conditions to produce a wave that propagates through the low-pressure section. Observations can be made in the flow behind the incident front or the reflected wave.

A Ludwieg tube is a cheap and efficient device for producing supersonic flow. It is a simple blow-down facility that operates somewhat like a shock tube. A large, evacuated dump tank is separated from the downstream end of a convergent–divergent nozzle by a diaphragm. The upstream end of the nozzle is connected to a long tube whose cross-sectional area is larger than the throat area of the nozzle. The initial pressure in the tube is high. When the diaphragm ruptures, a shock wave propagates into the low-pressure region, i.e., the dump tank. An expansion wave propagates into the high-pressure region, i.e., the tube with the nozzle. As the unsteady expansion propagates through the long tube, it sets up a steady subsonic flow toward the nozzle, which is accelerated by the convergent–divergent nozzle to a supersonic flow condition. The flow is constant until the expansion arrives at the nozzle again after reflection.

Figure 3 shows the schematics of a Ludwieg tube used for NICFD investigations, and the test section is shown in more detail for testing the flow through an annual turbine cascade [40]. This test facility was also employed for trailing edge flow investigations for an organic vapor with a high Mach number [41].

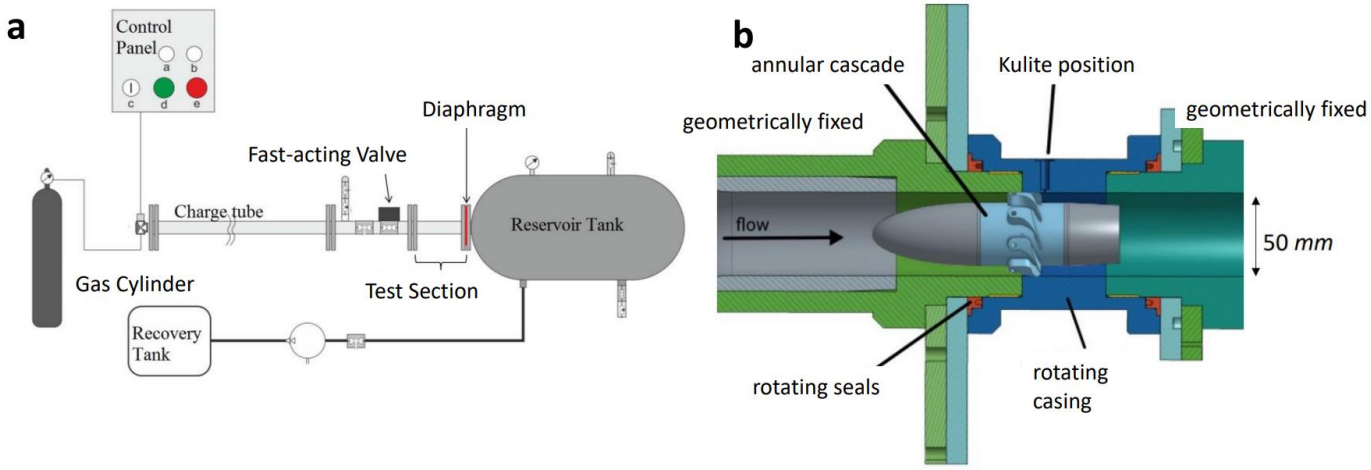

Figure 3. Ludwieg tube test facility for non-ideal compressible fluid dynamics investigations: (**a**) schematics of the tube; (**b**) details of the test section devoted to annular cascade testing. Pictures were taken from the web page of the Whittle Lab, Cambridge: https://whittle.eng.cam.ac.uk/lab/facilities/orc-ludwieg-tube/ (accessed date 15 December 2022).

Historically, the first use of a shock tube for investigating non-ideal compressible flow phenomena can be traced back to Fergason and Argrow [42]. In 2001, they attempted to demonstrate the existence of rarefaction shockwaves in PP10. The experiments were unsuccessful due to the thermal decomposition of the working fluid. Further technical problems finally led to the decommissioning of their shock tube facility. Some years later, in 2008, the group of P. Colonna completed the test facility FAST (Flexible Asymmetric Shock Tube) at the TU Delft [43]. The working fluid for this long tube (about 10 m) was D6. Expansion waves were measured, but non-classical gas dynamics were not observed. The challenges for performing such experiments were substantial, and, after the relocation of FAST to another building, further experiments were conducted [44]. A new attempt to prove non-classical gas dynamics has been recently published in [45].

In this context, the experiments [46,47] dealing with liquefaction shocks should be mentioned as well. The term liquefaction shock was introduced to distinguish it from the condensation of vapor in an expanding flow, i.e., the condensation shock. In a liquefaction shock, condensation takes place due to compression. Whereas such a phenomenon has not been observed for simple vapors such as steam or carbon dioxide, in organic vapors consisting of complex molecules, such a NICFD phenomenon can occur.

3.3. Blow-Down Wind Tunnels

In the 1960s, Duff [48] was probably the first to conduct CO_2 expansion experiments using a de Laval nozzle setup at the Gas Turbine Laboratory of M. I. T. that utilized a blow-down wind tunnel. The nozzle was fed by a bundle of nine 50 lb cylinders, thus enabling a testing time of about one minute. The work's objective was to better understand the condensation of various organic vapor flows in transonic and supersonic conditions to provide essential information for optimal turbine and power cycle space applications. A blow-down test rig for the investigation of supercritical CO_2 flow phenomena in a nozzle test section was employed at the same institution several years later [49].

A new blow-down wind tunnel, called TROVA (Test Rig for Organic Vapors), was designed in 2010 and erected at the CREA laboratory of the Politecnico di Milano to study the flows of dense organic vapors expanding from temperatures and pressures of up to 400 °C and 50 bar [50,51]. The first experimental results were presented in 2015 at the 3rd International Seminar on ORC Power Systems [52] and in 2016 at the 1st International Seminar on Non-Ideal Compressible-Fluid Dynamics for Propulsion and Power [53]. Figure 4 shows the schematics of TROVA. A power input of approximately 30 kW_{th} is sufficient to evaporate the organic vapor in the high-pressure vessel (see left side in Figure 4). The flow experiment is then carried out by opening a control valve. Measurement times of about 100 s can be achieved in the test section [54]. Typical test section throat areas are of the order 50 cm^2. The expanded vapor enters a condenser as a low-pressure vessel (see the right side in Figure 4). After condensation, the working fluid can be pumped back into the high-pressure vessel, and the blow-down testing can be repeated. The preparation time for an experiment is about a few hours. TROVA is equipped with instrumentation to record pressure and temperatures at relevant stations throughout the facility, and schlieren optical investigations or laser-optical measurement techniques can be applied (see Section 5).

During the same period, a blow-down configuration with a relatively small test section size was designed and commissioned by the group of Ricardo F. Martinez-Botas at Imperial College [55]. A 3.785 L cylinder was selected as the main blow-down vessel. Regulating valves were placed on either side of the test section, thus allowing a pressure ratio to be fixed across the measurement section. The selected working fluid was R1233zd (trans-1-Chloro-3,3,3-trifluoropropene), and the facility was designed for nozzle stagnation testing conditions of up to 20 bar and 138 °C, with a mass flow rate of 0.3 kg/s. The test section was a converging–diverging nozzle producing an expansion of Mach 2 at the exit plane. The purpose of the setup was to facilitate the validation of CFD software for the simulation of highly non-ideal flows. Thus, the relatively small size of the test section (the throat height of the nozzle was about 2 mm) was not too critical. The first results were reported in [56].

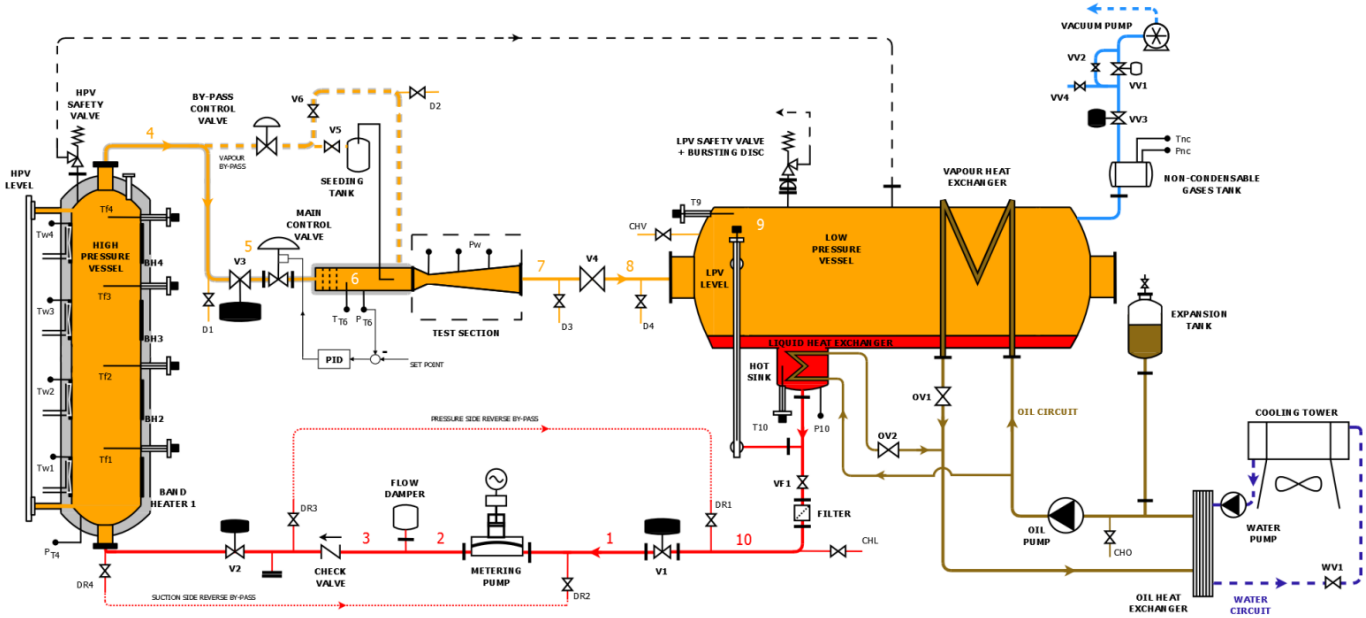

Figure 4. Schematics of the blow-down wind tunnel test facility TROVA [52].

3.4. Compressor-Driven Wind Tunnels

According to Dixon and Hall [57], "the design and performance prediction of axial flow compressors and turbines has been based, in the main, upon measurements of the flow-through two-dimensional cascades" using compressor-driven wind tunnels. The references [58,59] have been mentioned among the several available reviews of such conventional cascade wind tunnels. For testing the organic vapor aerodynamics of blades, a closed-loop wind tunnel driven by a compressor can be considered a natural test rig approach. However, such a concept's substantial power consumption for achieving high-speed flows is a disadvantage. Furthermore, compressor sealing must be carefully handled to avoid serious leakage flows. The entire device must be constructed as a pressure vessel to enable testing at elevated pressure and temperature levels. However, the great advantage of such a continuously running wind tunnel is the long measurement time.

The first generation of closed-loop wind tunnels working with non-ideal gases under highspeed flow conditions began in 1991. In a computational study [14], Anderson considered transonic airfoils in sulfur hexafluoride (SF6) and found that transonic similarity scaling could be used to relate results in SF6 to equivalent air results for primarily inviscid flows. NASA then began a program to convert a transonic wind tunnel into an SF6 operation to provide some experimental confirmation of Anderson's results. The schematics of this wind tunnel are shown in Figure 5. The test facility used for the current study was the 0.3-Meter Transonic Cryogenic Tunnel at the Langley Research Center [16]. The wind tunnel was operated at pressures up to 6 bar and temperatures from 100 K up to 300 K. Mach numbers from 0.15 up to 1.0 were achieved in the test section. The modifications required for operation with SF6 included a gas reclamation unit for charging and reclaiming the test gas, a gas analysis unit for real-time gas composition monitoring, a gas warning system for personnel safety, and a specially designed heat exchanger. The experiments demonstrated that transonic similarity theory was only partially successful in transforming the heavy gas results to equivalent nitrogen (air) results. After this test campaign, the test facility was decommissioned.

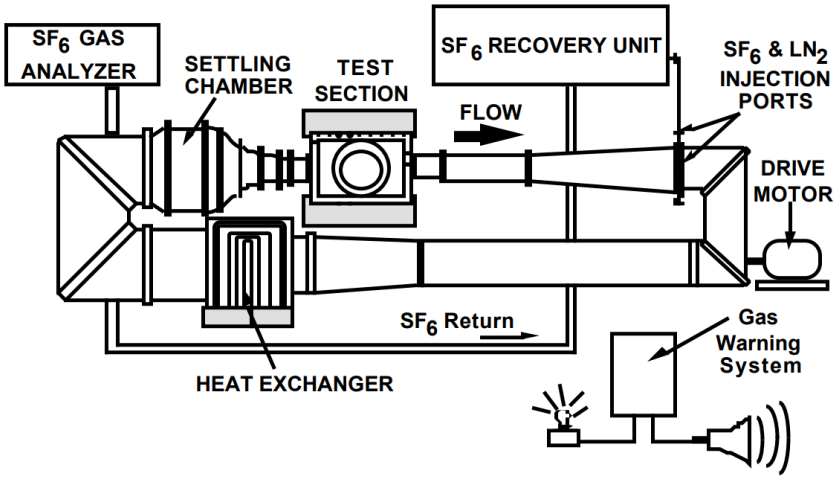

Figure 5. Schematics of the NASA transonic SF6 wind tunnel test facility (from [16]).

A new attempt to establish a transonic wind tunnel for organic vapors was published in 2015 by F. Reinker et al. [60]. This ORC vapor tunnel for continuous operation, called CLOWT (Closed Loop Organic vapor Wind Tunnel), is shown in Figure 6. Details about its design and operation features can be found in [61–63]. An application dealing with profile measurements of a linear transonic turbine cascade is described in [64]. For safety reasons, CLOWT has been operated with the non-toxic organic vapor Novec 649 by 3M. Due to the limited compressor power of about 65 kW, only high subsonic to transonic flows can be established in the test section. The minimum value for the fundamental derivative Γ is about 0.8.

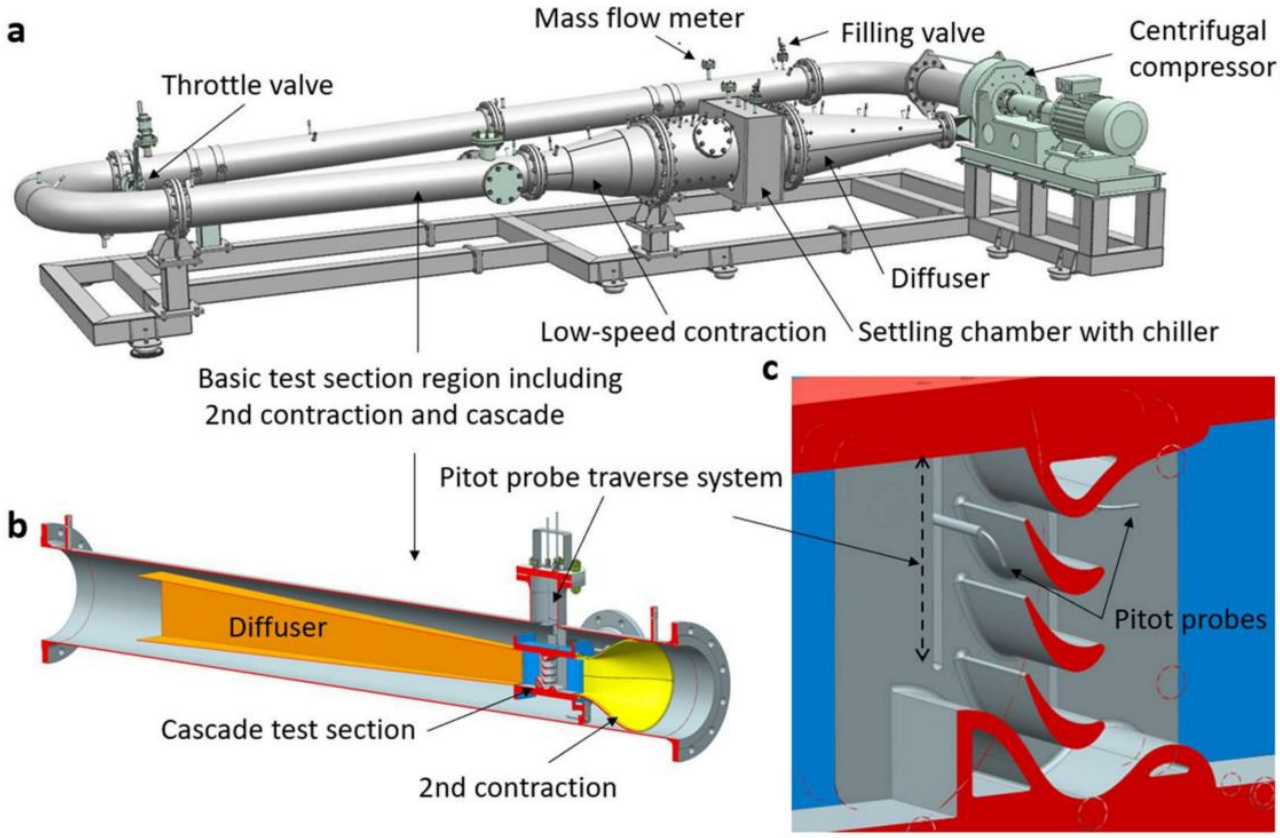

Figure 6. Test facility CLOWT (from [64]): wind tunnel (**a**), primary test section tube (**b**), and details of the cascade (**c**).

Also, White and Sayma [65] presented the preliminary design of a closed-loop supersonic test facility using a screw compressor. The facility's purpose was to provide experimental datasets of flows in a small test section under the same conditions as in ORC turbines. Initially, the selected working fluid was R1233zd, which was changed to R245fa. The facility was designed for testing conditions up to 20 bar and 125 °C, with a mass flow rate of 1 kg/s. As of the writing of this review paper, no experimental results have been published for this compressor-driven supersonic wind tunnel, although the rig has been fully pressure tested.

3.5. Rankine Cycle Wind Tunnels

A further approach to enable a continuous flow of vapor through a test section at elevated pressure and temperature levels is given by Rankine cycle wind tunnels. Here, the working fluid follows a Rankine cycle with the evaporator, test section (as a pressure-reducing or expansion component), condenser, and pump. This closed operational principal can be interpreted as a degenerated Rankine cycle, and the use of the expression "vapor tunnel" for this kind of test facility might be recommended. Replacing the test section with a turbine or another expansion engine turns such a facility into a test rig for power systems. To reduce the amount of heating power, an additional heat exchanger as a regenerator might be included. However, even then, the specific thermal power input required to operate the facility is substantial. The great advantage of such an approach is that high Mach number levels can be achieved with the benefits of a steady-state operation mode.

A Rankine cycle vapor tunnel was used in the early nozzle flow study [66] conducted by Bier et al. to investigate real-gas effects for R22 and other fluids. This experiment used a small Laval nozzle with a central static pressure probe as the test section. The throat dimensions were of the order of a few mm. Although the test section was small, relevant data could be obtained and compared with numerical predictions for the flow of non-ideal gases through a nozzle.

A hybrid high-temperature ORC vapor tunnel and expander test-bed was recently commissioned at the Aerospace Propulsion and Power laboratory of the Delft University of Technology [20,67]. The ORCHID (Organic Rankine Cycle Hybrid Integrated Device) test facility is shown in Figure 7. It was conceived for fundamental studies on NICFD flows and for testing ORC components, e.g., ORC turbines and heat exchangers. The ORCHID makes it possible, with its thermal power input of 400 kW_{th}, to attain a maximum temperature and pressure of up to 400 °C and 25 bar at the inlet of the test sections. It was designed to consider the possibility of using many different working fluids. MM (hexamethyldisiloxane) was selected for the first experimental campaigns, and corresponding results were published in 2021 [68].

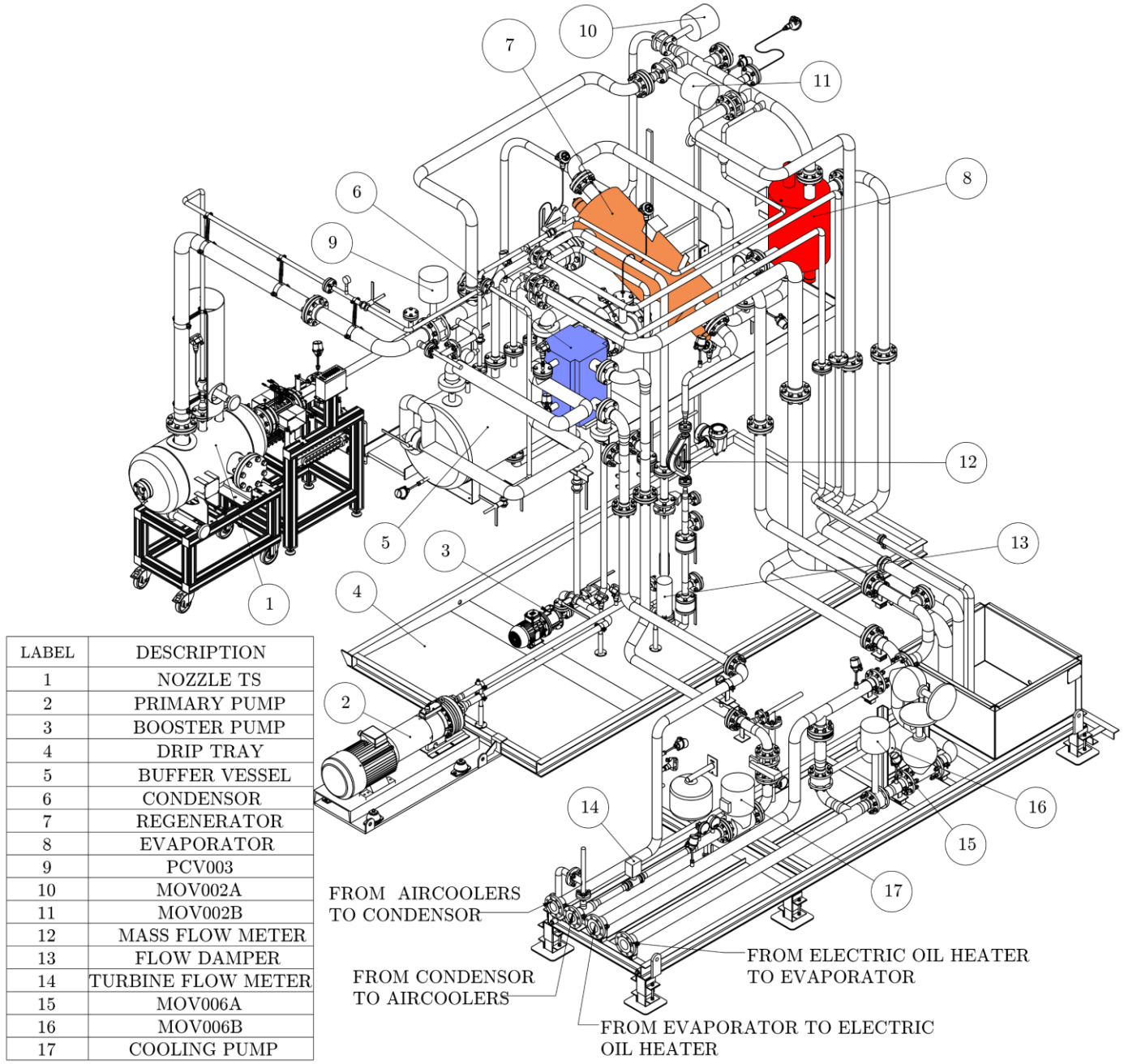

LABEL	DESCRIPTION
1	NOZZLE TS
2	PRIMARY PUMP
3	BOOSTER PUMP
4	DRIP TRAY
5	BUFFER VESSEL
6	CONDENSOR
7	REGENERATOR
8	EVAPORATOR
9	PCV003
10	MOV002A
11	MOV002B
12	MASS FLOW METER
13	FLOW DAMPER
14	TURBINE FLOW METER
15	MOV006A
16	MOV006B
17	COOLING PUMP

Figure 7. The Rankine cycle vapor tunnel test facility ORCHID [20].

3.6. Current Status of NICFD Test Facilities

Currently, all types of test facilities shown in Figure 2 are employed, and their complementary use enables valuable insights into non-ideal compressible fluid dynamics for a broad range of thermodynamic conditions. As of the writing of this review paper, several different NICFD test facilities, which were described above, are in operation [36,69]. To summarize, a list of their main parameters is provided in Table 3.

Table 3. Currently available NICFD test facilities (data obtained from a workshop organized by M. White, City University London [69]).

Test Facility	Institution	Type and Operation mode	Measurement Times	Working Fluids	Pressure	Temperature	Mach Number	Minimum Z/Γ	Test Section
TROVA	Milano, IT	Blow-down wind tunnel	10 up to 100 s	Siloxanes, refrigerants, hydrocarbons	Up to 50 bar	Up to 400 °C	Up to $Ma = 3$	$Z = 0.3/\Gamma < 1$	50 mm × 100 mm
ORCHID	TU Delft, NL	Rankine wind tunnel (continuously)	Long time	Siloxanes, refrigerants, hydrocarbons	Up to 25 bar	Up to 380 °C	Up to $Ma = 3$	$Z = 0.3/\Gamma < 1$	Limited by thermal power (400 kW)
CLOWT	FH Münster, DE	Closed wind tunnel (continuously)	Long time	Novec 649, air	Up to 10 bar	Up to 150 °C	Up to $Ma = 1.3$	$Z = 0.7/\Gamma = 0.8$	50 mm × 100 mm or 42 diameter (jet)
Cambridge Real-Gas Wind Tunnel	Whittle, UK	Ludwieg tube	10–100 ms	R134a, SF6, CO_2, Air, N_2, Argon	Up to 45 bar	15–150 °C	Up to $Ma = 2.5$	$Z = 0.6/\Gamma < 0.9$	50 mm tube diameter
ICL-TRANSIENT	Imperial, UK	Blow-down wind tunnel	Short time	Refrigerants	Up to 30 bar	70 °C (nominal)	Up to $Ma = 2.2$	$Z = 0.5/\Gamma = 1.05$	2 mm throat height

4. Pneumatic Measurement Techniques

Experimental investigation techniques for non-ideal fluid dynamics have been derived from the available methods of experimental fluid mechanics. The reader can find a general overview of these well-established techniques in [70–75]. A brief description of measurements in compressible flows of perfect gases is also included in [76,77]. This section and the following sections focus on the special modifications needed to apply some of these techniques to the aerodynamical investigations of organic vapors at elevated pressure and temperature levels. This review paper mainly considers techniques that are already in use or at a stage where valuable results have been reported in the literature. In Section 4, the pneumatic measurement techniques (i.e., pressure measurements) are discussed. Optical measurement techniques (i.e., schlieren pictures and laser optical methods, including PIV and LDV) are topics in Section 5. The hot-wire anemometry is the subject of Section 6.

4.1. Condensation Issues in Organic Vapors

The measurement of static and total pressures is fundamental for quantifying compressible flow phenomena. Pneumatic measurements are, furthermore, the key to loss determinations in turbine cascades [32,57].

The usual method for obtaining the static pressure of a flow along a wall is to drill a small hole that is normal to the surface of the wall and to connect this hole to a pressure transducer or manometer. Round nose or conical nose static pressure probes are also standard in subsonic and supersonic flows [77]. Total or stagnation pressures are measured through a Pitot tube invented by Henri Pitot in 1732 [78]. In a Pitot tube, the flow is isentropically brought to rest at the instrument's tip, where a small hole is placed. The hole is connected with a pressure transducer or manometer through a line. In addition to these two primary probes, combinations such as the Pitot static tube (also known as Prandtl probe) or multi-hole probes such as the five-hole probe are in use.

In the case of non-condensing air, pressure measurements are straightforward, but, in the case of organic vapors, where condensation can occur in the probes or the connecting lines, special care is required. The condensation of vapor within the pressure lines, tubes, or even in the probe can lead to the formation of an incompressible plug that effectively separates the transducer from the measurement location. This problem is referred

to as plugging or clogging, and it is common in multi-phase flow (e.g., droplet-laden air flows) or (wet) steam measurements [79].

In principle, three different approaches could be used to measure the pressures in a flow of an organic vapor at elevated temperature:

(i) The use of fully heated probes, lines, and pressure measurement devices to avoid any condensation;

(ii) The use of pressure transducers, in combination with lines added by liquid traps and purging devices, to remove condensate or liquid between the probes and the (cooled) measurement devices;

(iii) The use of probes and lines placed in the hot environment of the test rig while considering the condensation as a systematic error.

The first approach requires the use of measurement devices that are operable at higher temperatures. Although such a (mechanical) manometer solution might be available, its accuracy or resolution is typically too poor for accurate aerodynamic measurements. In the following discussion, it will be shown that only the second and third concepts have been employed so far for organic vapor flows.

The conventional approach is to purge the lines where condensation might occur (i.e., method (ii)). Murthy et al. [80] proposed a purge mechanism, in addition to the drain, to keep the probes and their ports dry for flow measurements in droplet-laden air flows. A purging approach for compressor cascades subjected to high fogging conditions was recently published in [81], which includes a discussion of the impact of the steadily applied purging pressure on the calibration curve and the pressure data interpretation. Purging with nitrogen (N_2) is common in droplet-laden air flows but is also used in vapor flows. Figure 8 details the pressure measurement method, which includes purging realized at the ORCHID test facility. Figure 8a shows the instrumentation of a nozzle test section with static pressure taps and their lines. The lines are related to the pressure transducers via a Scanivalve device, which includes liquid traps (see Figure 8b) and an additional tank filled with the purging gas (N_2). The condensate can be observed in the liquid traps equipped with optical access (see Figure 8c), and the purging process can be initiated. The impact of purging on the measurement signals is shown in Figure 9. Significant peaks can be observed in Figure 9a that indicate the purging blow. Figure 9b is a schlieren picture of the nozzle test section during a purging event.

A pneumatic system for pressure measurements in the transient flows of non-ideal vapors that are subject to line condensation for the TROVA blow-down wind tunnel was presented in 2021 by Conti et al. [82] (see Figure 10). The rectangular boxes in Figure 10 represent pressure transducers. The purging fluid is N_2. Further details about the pressure measurement system, including Pitot probes, can be found in [83,84]. The central concept is essentially based on two lines: one exiting the plenum for the total pressure determination of the wind tunnel, and one connected to the probe tap measuring the total pressure at the test section location. Both lines are directly connected to a nitrogen storage tank. Electrical actuator valves were employed to open, as the test was triggered to flush lines with nitrogen at a pressure slightly higher than the expected maximum level during the test and close right after the pressure peak was reached in the test section during the experiment.

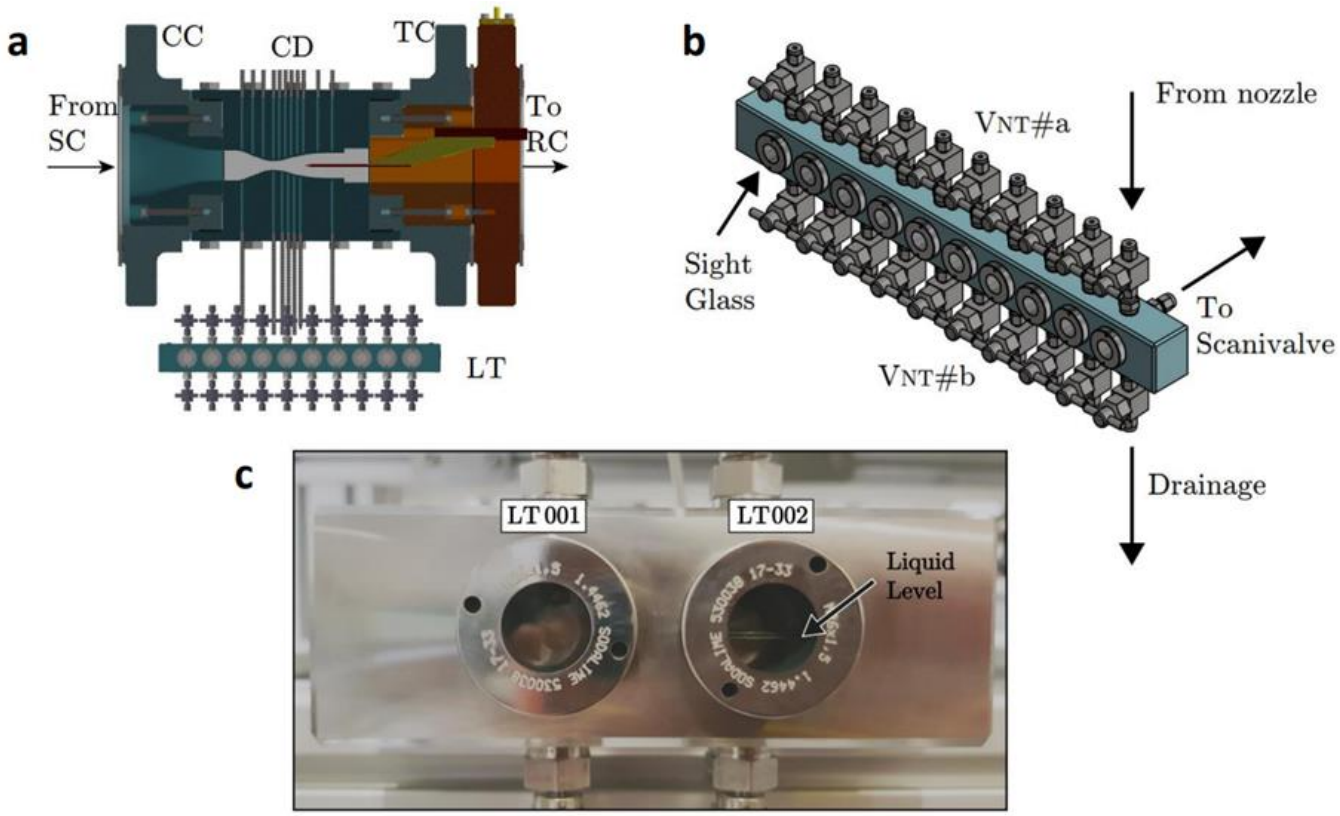

Figure 8. Pressure measurement system including liquid traps and purging realized at ORCHID (from [20]): (**a**) cross-section of the nozzle housing (SC: settling chamber; CC: contraction channel; CD: converging-diverging nozzle: MSC: model support compartment; PT: pressure taps; LT: liquid traps; RC: receiver); (**b**) assembly of the liquid traps (valve VNT#a isolates the process from the Scanivalve, valve VNT#b allows the liquid to drain during operation); (**c**) observation of condensate in a liquid trap indicating the need to purge.

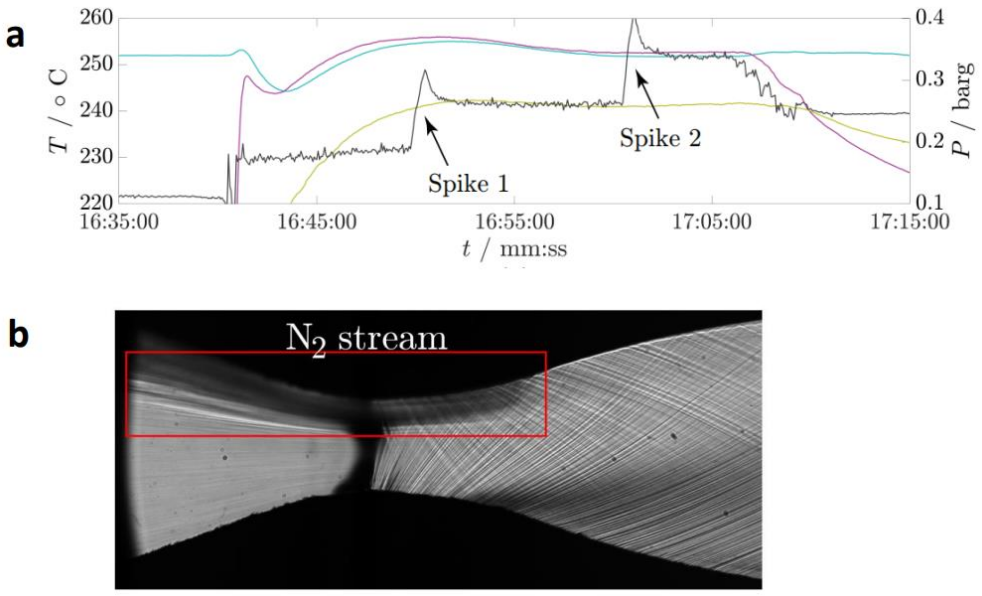

Figure 9. Impact of purging on nozzle flow measurements: (**a**) two spikes in the pressure signal due to purging of the liquid traps by means of nitrogen injection in the lines; (**b**) schlieren image showing a stream of N_2 being convected through the nozzle (from [20]).

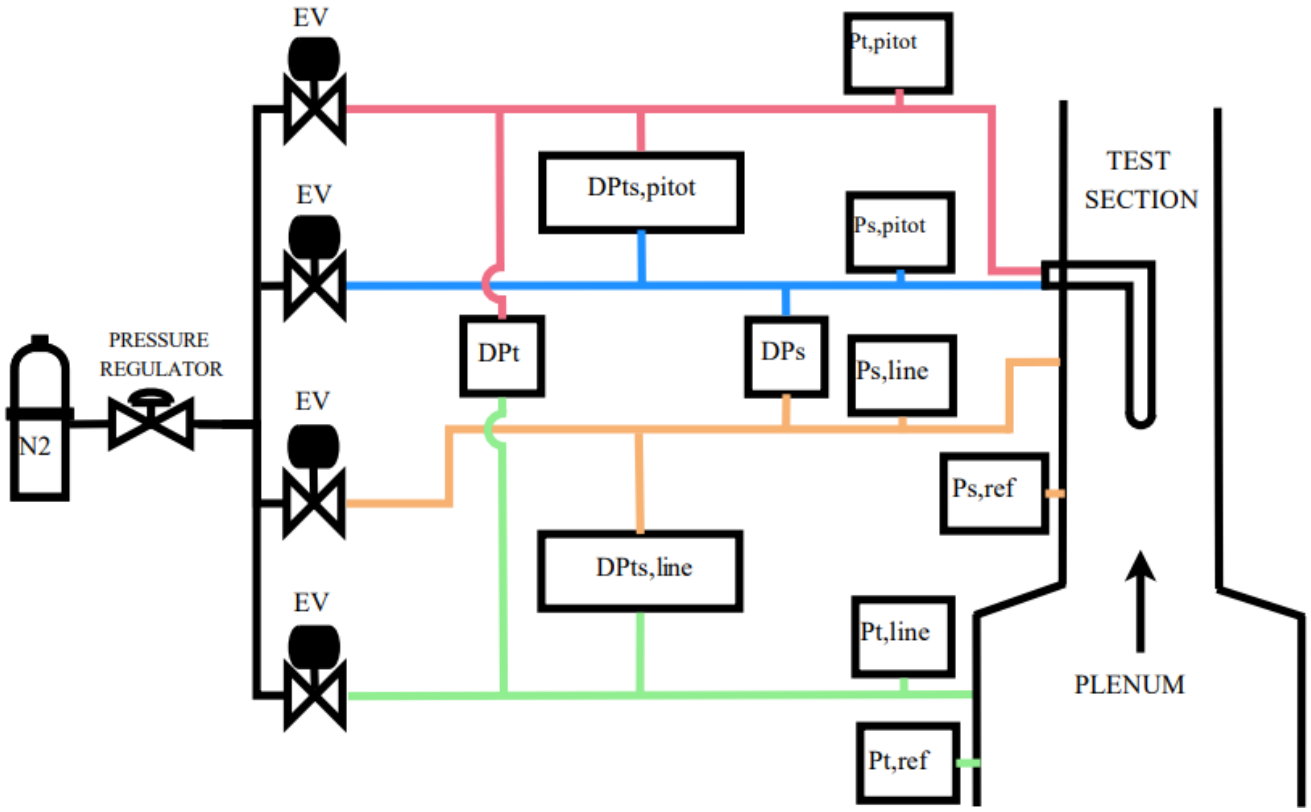

Figure 10. Flushed pneumatic lines scheme for Pitot tube testing in subsonic flows of Siloxane MM in the TROVA blow-down wind tunnel (from [82]).

This procedure ensures that each line contains only nitrogen during a test and that no MM vapor enters a line. Hence, no condensation in the nitrogen-filled lines can occur. As the test proceeds, nitrogen exits the line through the static tap into the test section, as the line pressure is in equilibrium with the decreasing test section one. Figure 10 also shows the differential pressure transducers used to obtain static and total pressures at different locations in the wind tunnel.

Whereas adding nitrogen to the working fluid is not a severe issue in test rigs employing evaporators and condensers (because the non-condensable gas N_2 can be separated from the vapor condensate), a different strategy should be chosen in the case of continuously running closed-loop organic vapor wind tunnels to avoid significant contamination of the working fluid. Hence, an alternative approach was chosen for the compressor-driven closed-loop organic vapor wind tunnel CLOWT to handle the condensation issue. The method employed by Reinker et al. [85] in 2020 and used in other studies, e.g., [64,86], was to place the valves and pressure lines in the heated area of the wind tunnel where no condensation could occur (see Figure 11). By using a valve system operated by a rotative mechanism (shifter), twenty pressure taps or probes could be connected to an external transducer at room temperature (Figure 11a). This transducer was thermally decoupled from the hot lines by utilizing a curved metal tube. The ambient room temperature of the laboratory hall cooled down the external tube up to room temperature at the end where the transducer was connected. Hence, the organic vapor resting in the pressure line condensates and fills the liquid trap up to the level where the liquid can flow back due to gravity. The position of the liquid can be seen as a cold area in the thermography (Figure 11b). The surface tension of the working fluid Novec 649 is relatively low, and no severe plugging can occur in sufficiently large tubes. Since the saturation pressure of Novec 649 at room temperature is low (T_{sat} = 49 °C at p = 1 bar), the pressure in the test section presses the liquid to the transducer. As a systematic measurement error, the hydrostatic pressure in the liquid trap occurs if the exact position of the liquid level is not

known. This systematic pressure can be minimized by designing traps with small heights. External temperature measurements along the trap enable a further estimation of the liquid column height in the device (see Figure 11b).

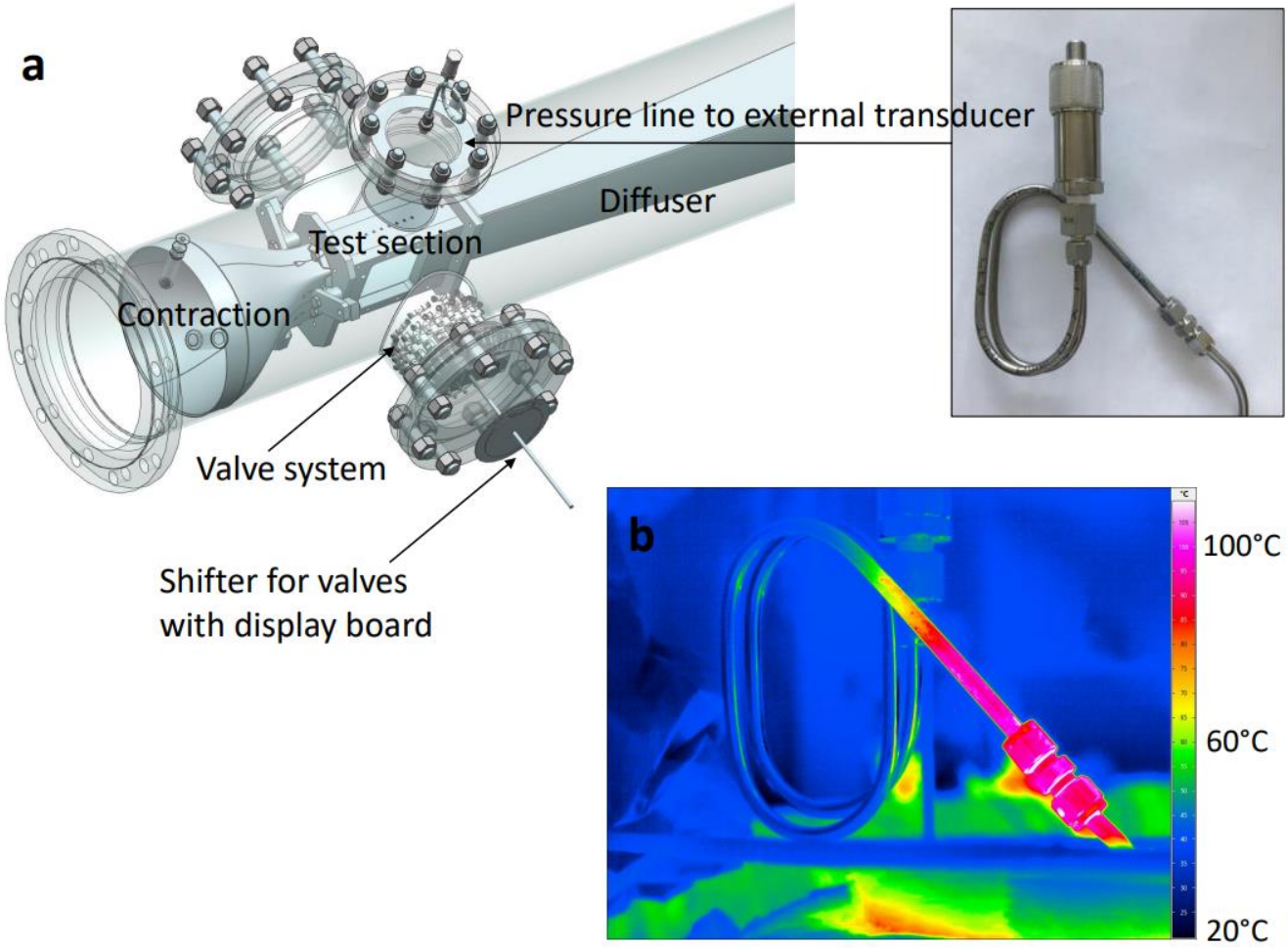

Figure 11. The pressure measurement system realized at the CLOWT closed-loop wind tunnel: (**a**) valve and lines placed in the hot domain of the primary test tube and (**b**) thermography of the thermally decoupled transducer indicating the region of liquid trapped in the line.

It should be remarked that an approach without purging requires a long preparation time to achieve a thermal equilibrium in the entire system. Furthermore, very low test section pressure levels, below the saturation pressure at transducer temperature, might not be measured accurately by such an approach. In the case of very short measurement times in shock tube experiments [41], fast pressure sensors can be used directly without purging devices. Details about such an application can be found in [87].

4.2. Pitot and Stagnation Pressure Probes

Shortly after the commissioning of wind tunnels for organic vapor flows, research efforts started to move towards using pressure probes for non-ideal compressible flows. The first use of a stagnation probe for investigating non-ideal compressible flows was reported in 2015 [41,87]. To capture the wake measurements of an idealized trailing edge configuration, a probe with four "Kulite XCL-62" pressure transducers was placed downstream of a trailing edge in the test section of a Ludwieg tube (see Figure 12). The probe was produced using laser sintering 3D printing. The design was a wedge probe configuration with a wedge angle of 10 deg, which widened slightly at the base to accommodate the sensors inside. The sensors were mounted within the probe to ensure minimal

response times. Furthermore, the setup shown in Figure 12 employed an inlet stagnation probe.

In 2020, the first detailed performance study [85] of a rotatable cylinder Pitot probe in high subsonic flows of Novec 649 was published. Due to the choking effect caused by the cylinder Pitot probe (diameter 5 mm) in the closed test section (50 mm × 100 mm), the maximum inflow Mach number was about Ma = 0.7 in the study [85]. Later, the same configuration was used for detailed profile pressure measurements and drag coefficient determinations of a cylinder subjected to high subsonic streams of Novec 649 [88].

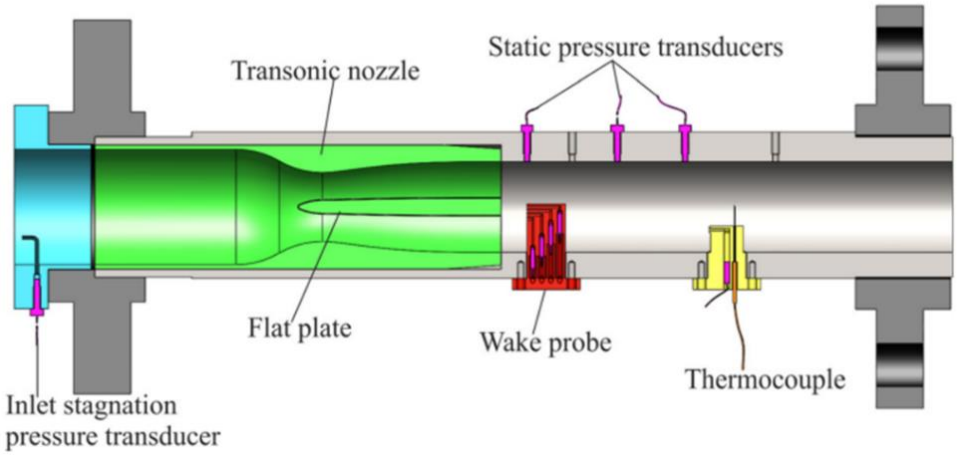

Figure 12. First use of a stagnation probe ("Wake probe") for non-ideal compressible flow (from [87]). The setup might be compared with the one shown in Figure 3.

Applications of a Pitot probe for shock losses at a supersonic flow of MM were published by Conti et al. [82,84] and by Manfredi et al. [89,90] in 2021 and 2022. The Pitot probe design used in these studies is shown in Figure 13. The Pitot probe measurement concept used the purging system discussed in the previous subsection (see Figure 10). In these studies, schlieren pictures of the shock caused by the probe in the supersonic flow were shown as well. It was found that, even at mildly non-ideal conditions with $Z \gtrsim 0.70$, non-ideality was responsible for a significantly stronger shock than the ideal gas at the same pre-shock Mach number [84].

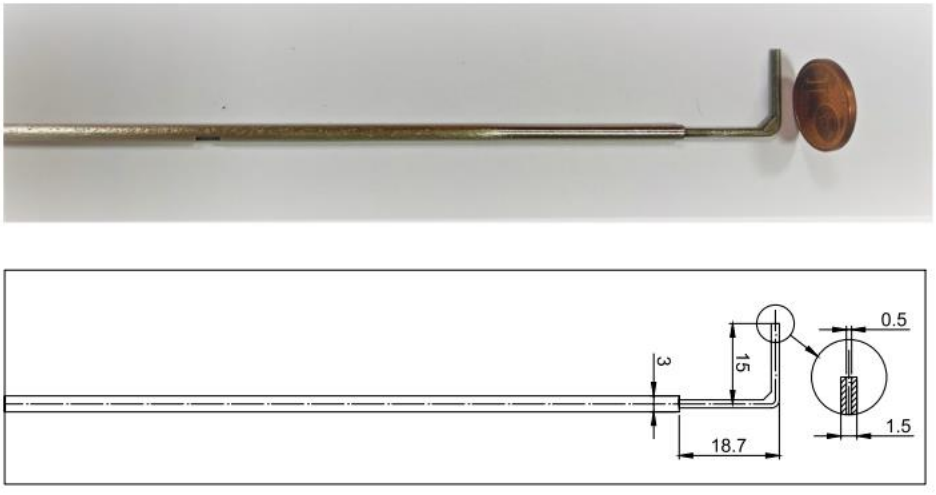

Figure 13. Pitot probe used in the shock loss experiments by Conti et al. [82,84]. Dimensions in mm.

4.3. Blockage Effects and Probe Interaction

The problem of probe interaction with the flow to be investigated can be substantial, especially in supersonic flow. Figure 14 illustrates that issue by comparing two computational fluid dynamics simulations for a conventional round probe and a wedge probe in the flow downstream of a supersonic cascade. The traditional design of the probe introduces a significant disturbance. Based on the CFD results, a wedge probe design was manufactured and successfully employed [91]. In general, wedge probes are recommended for supersonic flow investigations due to their more minor probe interaction effect.

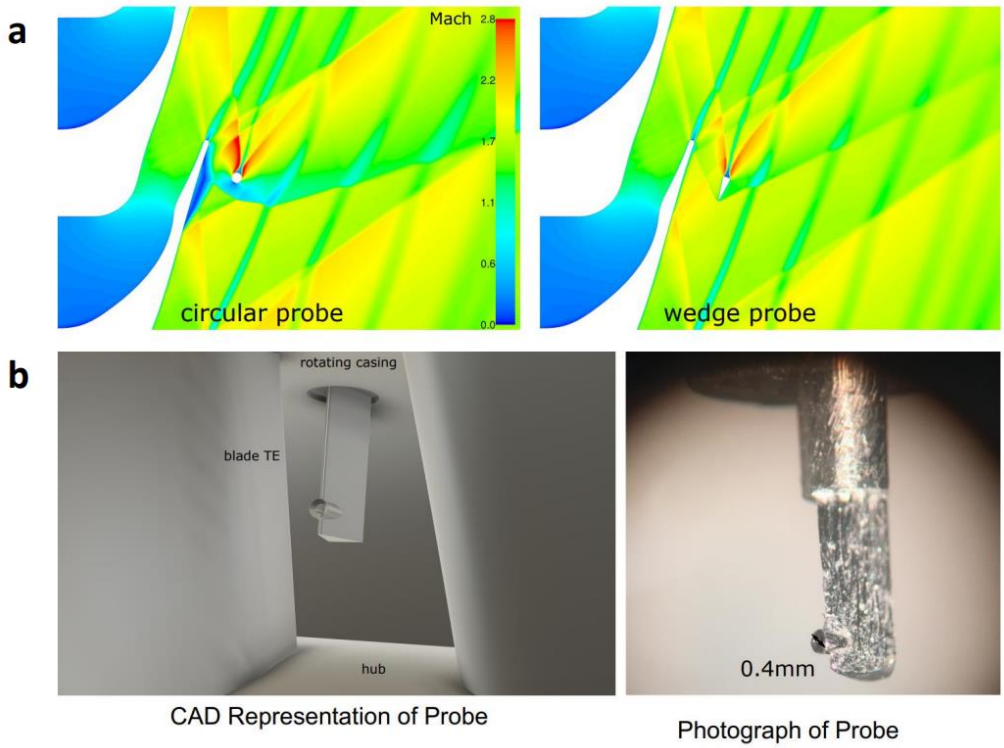

Figure 14. Illustration of probe interaction problems (**a**) and design of a wedge probe for total pressure measurements downstream of a turbine cascade (**b**). The Mach number level is indicated by the color bar at the top. The pictures were taken from [91].

Blockage and probe interaction effects can be substantial and can noticeably affect the data reduction process. Although non-ideal compressible flow dynamics would require a modification of corresponding ideal gas relations, the order of magnitude of blockage corrections might still be assumed to be valid. Blockage corrections for cylinder probe calibrations were proposed by Wyler [92] based on an ideal gas analysis and similitude considerations. He found that the blockage effect in free jets was found to be approximately the same magnitude as in closed tunnels. Truckenmüller et al. [93] reported probe blockage effects for transonic flow through a calibration wind tunnel and a guide vane row in a three-stage model turbine. It was found that even a probe placed downstream of a cascade could noticeably influence the blade profile pressure distribution of the cascade. Related studies on that topic include [94,95]. So far, a detailed experimental investigation of non-ideal compressible flow dynamics on probe interactions is missing.

4.4. Pressure Data Reduction for NICFD

The static wall pressure is usually obtained through small holes drilled in the wall and connected to a manometer. Ducruet [96] pointed out the possible impact of the boundary layer, velocity gradient, and wall curvature on this kind of measurement. However, correction schemes are uncommon in practice.

The theory of Pitot probes and the corresponding data reduction process for total pressure are well-treated in textbooks [76,77] for perfect gases. In the case of an ideal gas with an isentropic exponent γ, the famous Rayleigh–Pitot equation

$$\frac{p_{o2}}{p_1} = \frac{\gamma+1}{2} Ma_1^2 \left(\frac{(\gamma+1)^2 Ma_1^2}{4\gamma Ma_1^2 - 2(\gamma-1)} \right)^{1/(\gamma-1)} \tag{16}$$

results in the case of supersonic flow. Here, p_{o2} denotes the measured total pressure at the probe hole, and p_1 and Ma_1 are the static inflow pressure and Mach number, respectively. For subsonic flow, the isentropic relation

$$Ma_1^2 = \frac{2}{\gamma-1} \left(\left(\frac{p_{o1}}{p_1} \right)^{(\gamma-1)/\gamma} - 1 \right) \tag{17}$$

can be used to determine the inflow Mach number for a perfect gas. In subsonic flow, there is shock caused by the probe, and the inflow total pressure p_{o1} can be measured directly.

In the more general case of non-ideal compressible flow, the data reduction process must start with the general balance equations

$$\rho_1 c_1 = \rho_2 c_2, \tag{18}$$

$$h_1 + \frac{1}{2} c_1^2 = h_2 + \frac{1}{2} c_2^2 = h_0, \tag{19}$$

$$p_1 + \rho_1 c_1^2 = p_2 + \rho_2 c_2^2 \tag{20}$$

and assumes an isentropic process. Together with an appropriate equation of states, the inflow Mach number Ma_1 or other quantities can then be computed based on the measured probe pressure and the total inflow state. As pointed out by Spinelli et al. [97], in a non-ideal compressible flow, the expansion process depends on the inflow state, whereas the perfect gas relations (16) and (17) do not. Furthermore, the shock pattern caused by the probe can differ. An illustration is shown in Figure 15 where schlieren pictures of the shock caused by a Pitot probe placed in a supersonic flow of nitrogen (perfect gas) and MM (non-ideal organic vapor) are compared.

A simple routine for Pitot probe data reduction was published in [98]; alternative mathematical schemes to handle normal shock under non-ideal compressible flow conditions were discussed by Passmann et al. [99]. The essential parts of the data reduction are the correct and efficient method to compute the isentropic flow relations and to solve the non-linear set of governing equations [98,99]. In [84], the data reduction was performed by numerically solving mass, momentum, and energy conservation equations across the shock, coupled with the Span–Wagner thermodynamic model through the FluidProp library [100]. This multiparameter model provides accurate thermodynamic properties, even close to the critical point. A functional form, in terms of the reduced Helmoltz free energy as a function of the inverse reduced temperature and reduced density, is provided for the fundamental relation linking all thermodynamic properties of a simple system in a stable equilibrium state. For the working fluid in [84], siloxane MM, appropriate model parameters were reported by Colonna et al. [101,102], and further information can be found in [103,104].

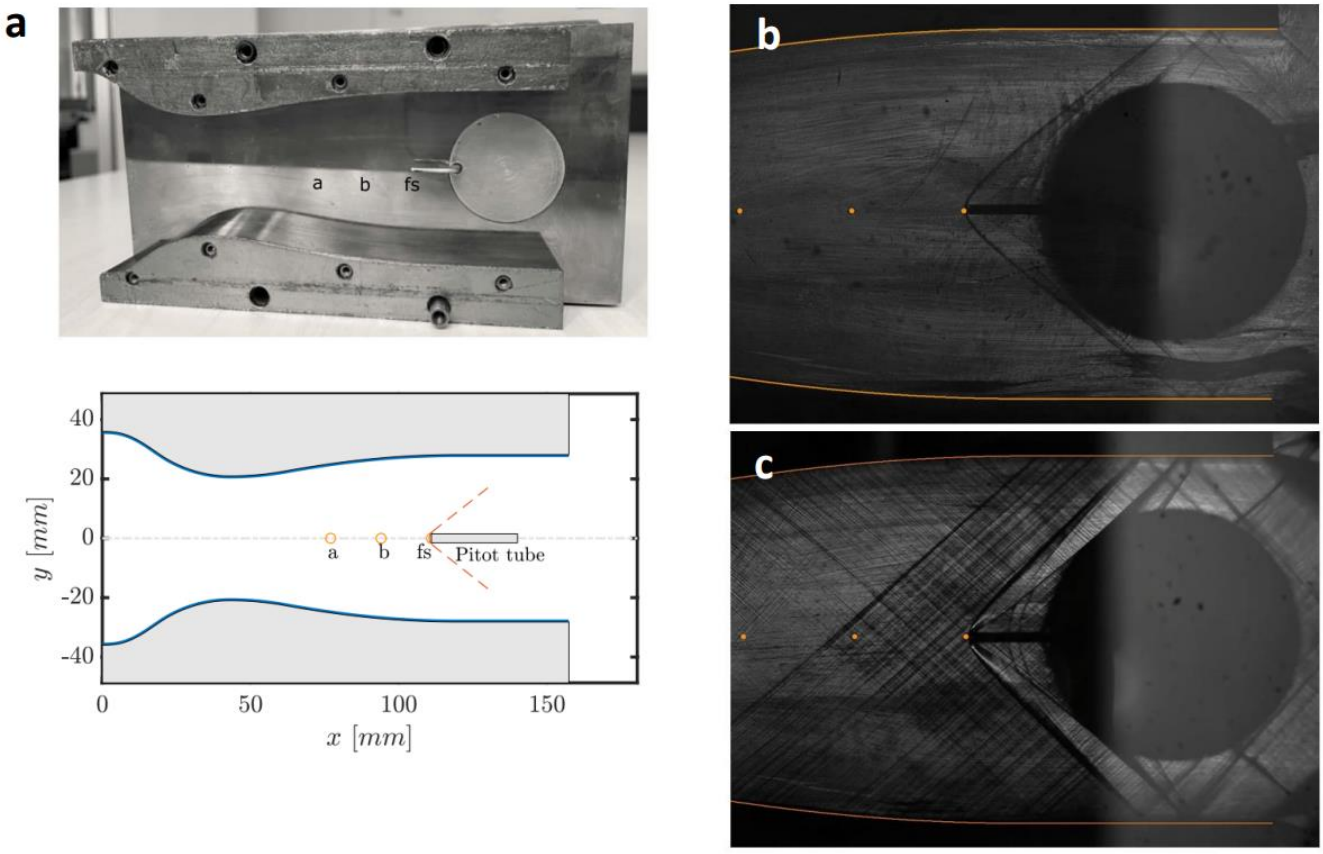

Figure 15. Demonstration of shocks caused by a Pitot probe placed in supersonic flow (from [84]): (**a**) flow nozzle with pressure taps (a, b, and free stream fs) and Pitot tube with a bow shock sketch; (**b**) schlieren image for flow of N_2; (**c**) schlieren image for flow of MM with $Z = 0.70$; the nozzle profile and pressure taps are highlighted in the schlieren pictures.

The need to employ suitable equations of states and to replace the classical formulas (16) and (17) for non-ideal compressible fluids is illustrated in Figure 16. Here, the Mach number obtained by the perfect gas relation and an adequate data reduction scheme for Novec 649 are compared. As indicated by Figure 16, even for moderate Mach number levels, the error between the perfect gas routine and the non-ideal data reduction can be 6%. Much larger errors can occur at higher Mach number levels and at the dense gas regime [98,99].

If fast measurements have to be performed, the transient behavior of the entire system must be considered. A corresponding analysis was proposed by Gori et al. [105]. In this work, it was found that the step responses depended on the speed of sound of the working fluid, thus indicating that molecular complexity plays a significant role in determining the promptness of the measurement devices.

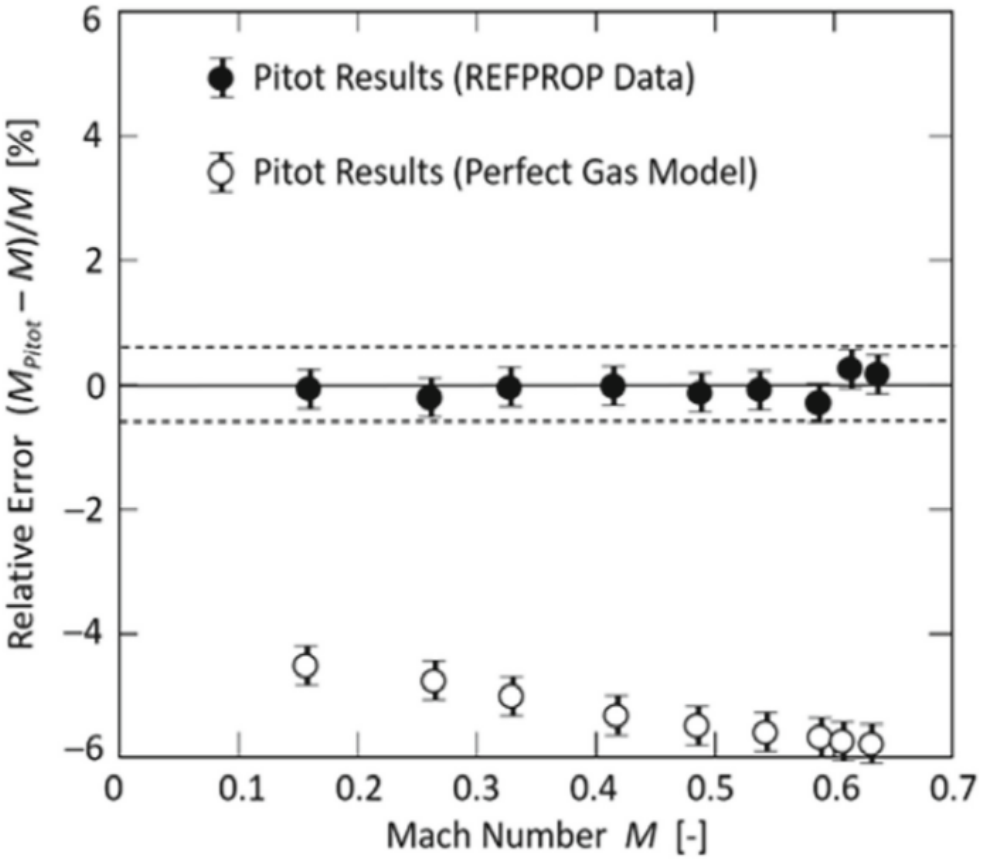

Figure 16. Relative error of Mach number calculations based on Pitot probe data and thermodynamic models for the subsonic flow of Novec 649 (from [85]).

5. Optical Measurement Techniques

Optical flow measurement techniques are widely applied in science and engineering applications [72–75]. This section briefly reviews the currently available and employed methods for non-ideal compressible flow dynamics. This includes discussing schlieren methods and laser-based measurement techniques (particle image velocimetry PIV and laser Doppler velocimetry LDV). A comprehensive presentation of optical techniques (i.e., schlieren and LDV) that were applied within the TROVA facility at the CREA laboratory of Politecnico di Milano is found in [106]. A feasibility study, limited to low-speed flows of PIV for NICFD applications, was published by Head et al. [107].

5.1. Schlieren Optical Methods

The classical experimental tool in gas dynamics is, since the pioneering work of Ernst Mach (see [77]), the schlieren image method. Schlieren images easily provide qualitative data, and they can also provide quantitative data about the local Mach number and instantaneous slope of shock waves. Settles [108] presented the history of the schlieren instrument and a very detailed account of its various technical details. The origin of this instrument can be traced back to the 17th century, when Robert Hooke used a primitive device to illustrate the thermal convection from a candle flame. In the 19th century, Toeppler brought the instrument to a practical and valuable level. Since his work, the German expression "schlieren" has been used. It might be remarked that "schlieren" is not a name of a person (although in the German language, it is written with a capital S); it is the German word for "streak."

Since organic vapors are transparent, applying schlieren systems to NICFD investigations is relatively straightforward. With the schlieren system, density variations and,

thus, index-of-refraction variations can be visualized within a transparent medium like a gas or a vapor. Regarding NICFD applications, three schlieren systems, which are schematically shown in Figure 17, have been used so far: (a) the conventional z-type schlieren systems, (b) the double-pass schlieren system, and (c) the background-oriented schlieren method. A fourth method (d) is the focusing schlieren system approach. The latter has not been applied to NICFD investigations so far. For a description of the physics of schlieren and shadowgraph techniques, the reader can consult [108] or [109].

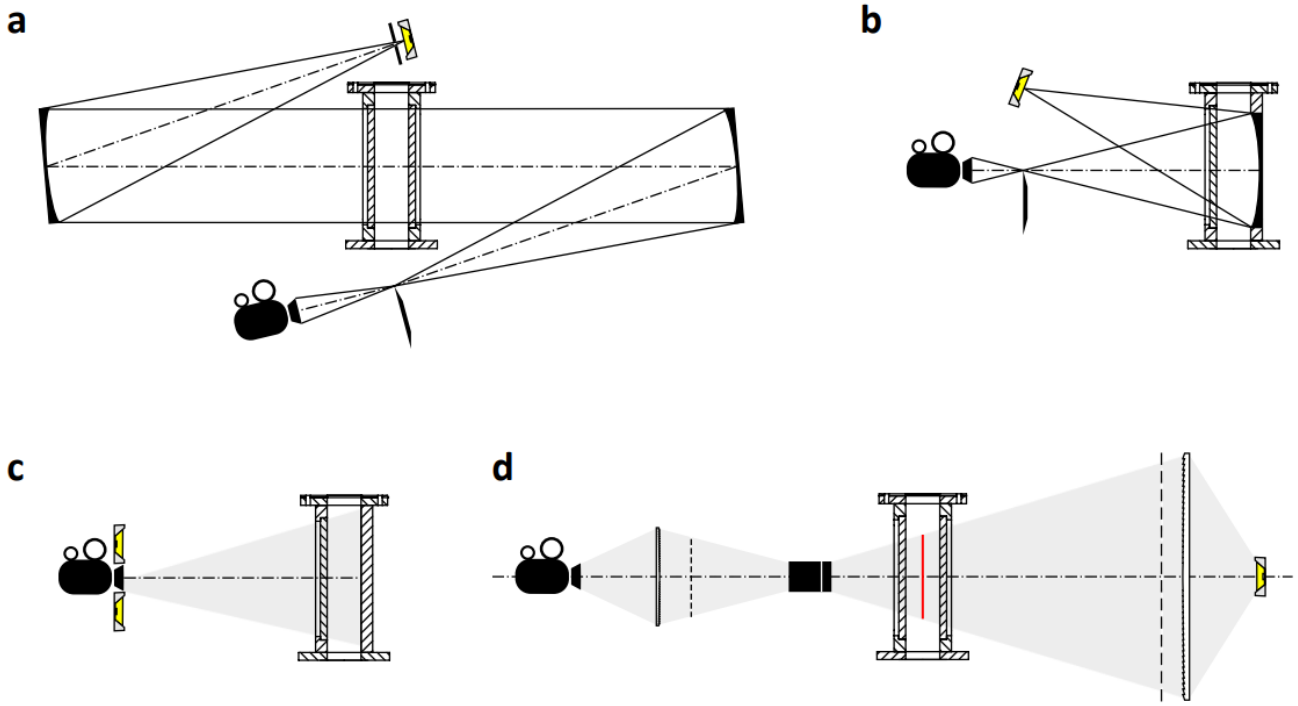

Figure 17. Schematics of schlieren systems for NICFD investigations: (**a**) conventional z-type schlieren system. (**b**) double-pass schlieren system. (**c**) background-oriented schlieren system. (**d**) focusing schlieren system.

The z-type, two-lens configuration was used in schlieren image experiments conducted by Head [20] in the ORCHID test facility. However, the first schlieren results for a non-ideal compressible nozzle flow were presented by Spinelli et al. [52] in 2015, and they employed a double-pass system. A double-pass-type parallel light schlieren system with the emitting and receiving optical components mounted on an optical table was used in this first study, because this configuration is shorter and easier to align with respect to the classical z-type system. The schematic of the employed approach is shown in more detail in Figure 18.

A 100 W Hg arc lamp was used in [52] as the light source, which was focused by an F/1.5 silica lens into a circular spot of about 3 mm in diameter and then collimated to form parallel light rays by a schlieren lens head (Lens 1 in Figure 18). The latter had a diameter of 150 mm and a focal length of 1000 mm. The collimated light beam was deflected by a circular mirror (Mirror 1 in Figure 18) before traversing the test section. It was then reflected by the schlieren head by the metallic mirror "0", which was the polished nozzle back wall. Then, the beam was focused on the vertically aligned knife edge. The knife orientation made it possible to visualize the density gradient along the nozzle axis. A cubic beam splitter (prism) separated the light beam originating from the light source and the reflected one. A lens of 160 mm focal length and 50 mm diameter was located behind the knife (Lens 2 in Figure 3), and created a real image of the test section on the sensor of a high-speed camera. The camera resolution and frame rate were set to 1024 × 512 pixels

and 100 fps (frames per second), while the exposure time was set to 20 μs. The use of a mirror-polished rear plate was cost-efficient, and its optical quality was high enough to ensure no significant disturbances in the schlieren images. However, a polished surface gets dirty quickly, so it must be cleaned every few tests to achieve good contrast and sharpness in the schlieren images. Usually, some drops of liquid working fluid or isopropyl alcohol are effective cleaning fluids. The same procedure can be used to clean quartz windows. The reflectivity of the stainless-steel plate is affected by the siloxane vapor, which the light source intensity might compensate for. Later, LED light sources became popular for schlieren systems.

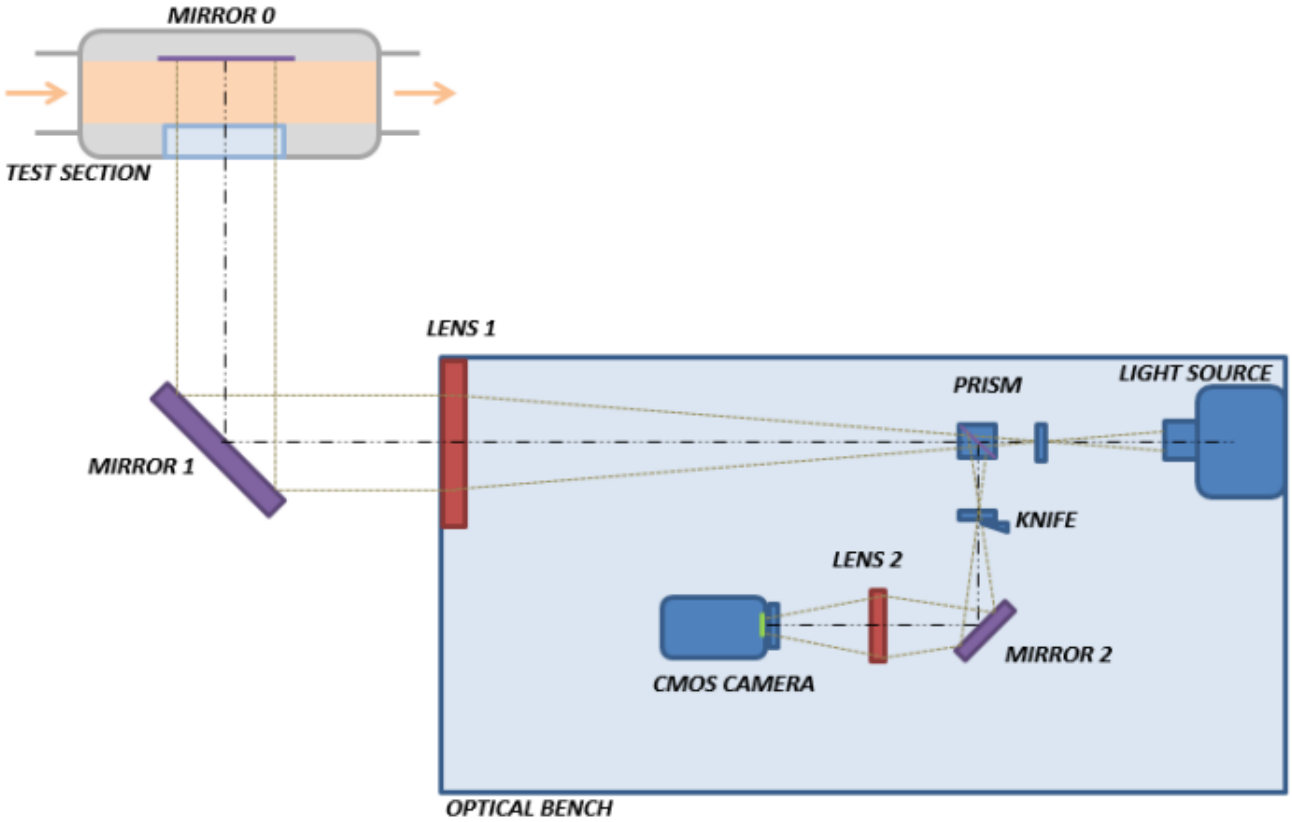

Figure 18. Schematic of the double-pass schlieren system employed by Spinelli et al. [110].

Figure 19 shows the first results obtained in [52] for a nozzle flow of MDM. Condensation of the MDM vapor occurred along the back plate, which was not heated. Condensation prevented the use of the double-passage schlieren techniques, since liquid drops and film that flowed over the back plate produced reflected rays featuring high optical distortions (see Figure 19a). That outcome prevented the detection of the density gradients in the vapor phase. Direct observation of the test section revealed that condensation occurred only along the metal plate. When the vapor flow heated the test section, the liquid film evaporated. Then, oblique shock waves originated immediately after the recessed step became visible (with their reflection at the contoured wall), thus confirming the occurrence of a supersonic flow of MDM vapor within the nozzle (see Figure 19b).

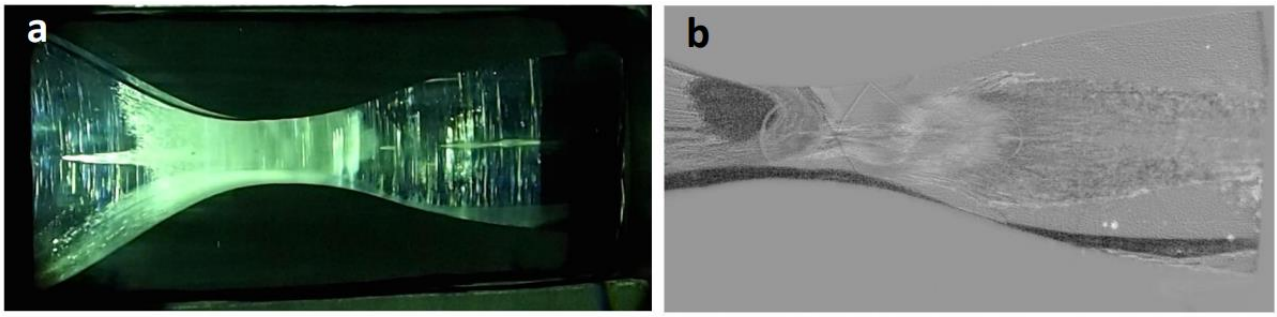

Figure 19. Pictures of the test section during the first experimental runs with MDM in 2015 (from [52]): (**a**) condensation along the back plate and formation of a liquid film in the convergent section of the nozzle (**b**) schlieren visualization of the oblique shock waves at a later experimental run.

In the following studies [97,110], the quality of the schlieren pictures obtained by the double-pass system was improved. Figure 20 shows a schlieren picture with Mach lines that enable the determination of the Mach number along the nozzle expansion path. The actual Mach number Ma can be determined from the observed angle α (enlarged by the central green lines in the top picture of Figure 20) by the relation

$$Ma = \frac{1}{\sin \alpha} \tag{21}$$

The detection of Mach lines according to Equation (21) permits a direct measurement of the local Mach number without involving any thermodynamic model in the calculation if the flow direction is known. A detailed description of the algorithm is reported in [111]. The comparison with the prediction of a computational fluid dynamics (CFD) simulation of the nozzle flow was in good agreement (see Figure 20).

Steady oblique shock waves were observed for the first time in the non-ideal supersonic flows of a single-phase organic vapor in 2019 by Zocca et al. [112]. A diamond-shaped airfoil with a semi-aperture of 7.5° at the leading edge and 10° at the trailing edge was placed within a uniform supersonic stream (Mach number Ma = 1.5) of siloxane MDM. The measurements demonstrated the dependence of the pressure ratio across the shock on the applied stagnation conditions for a non-ideal compressible flow. Schlieren pictures for a nozzle-arrangement-based airfoil with vanishing deflection were obtained by Manfredi et al. [89,90] and presented in 2022.

In addition to the schlieren images obtained by z-type or double-pass systems, the background-oriented schlieren (BOS) technique permits the visualization of small density gradients. Since the light rays deflect when passing through fluids with different densities, the BOS technique can detect the resulting refractive index gradients as integrations along a line of sight. In [113], a corresponding system was proposed for supersonic flow applications. Further applications of the BOS technique can be found, for instance, in [114–120]. The schematics of a BOS system are already shown in Figure 17c. The first application of a BOS system for a non-ideal compressible flow was presented in 2022 by Sundermeier et al. [121]. In this work, the high subsonic flow (Ma = 0.65) of Novec 649 through a circular cylinder was investigated. The principle and some results, including the comparison with the outcome of a Large Eddy Simulation (LES), are shown in Figure 21. As a datum or reference image, the test section without any flow was considered. Suppose fluid flows through the test section with density gradients, distortions, or schlieren results. Using the reference picture, a density or schlieren picture can be computed in a post-processing step. This is illustrated in Figure 21. Local shocks caused by the trailing edge of the cylinder and the von Karman vortex street downstream of the cylinder can be observed. Based on the distances of the vortex cores, the corresponding Strouhal number was computed and compared with the LES results. It was found that the vortex shedding frequency (i.e., the Strouhal number) was nearly constant (at about 0.20), and it was independent of the

Reynolds or Mach numbers. Although locally, the non-ideal gas behavior affected the shock pattern and the location of the shocks, the vortex shedding was relatively stable and robust.

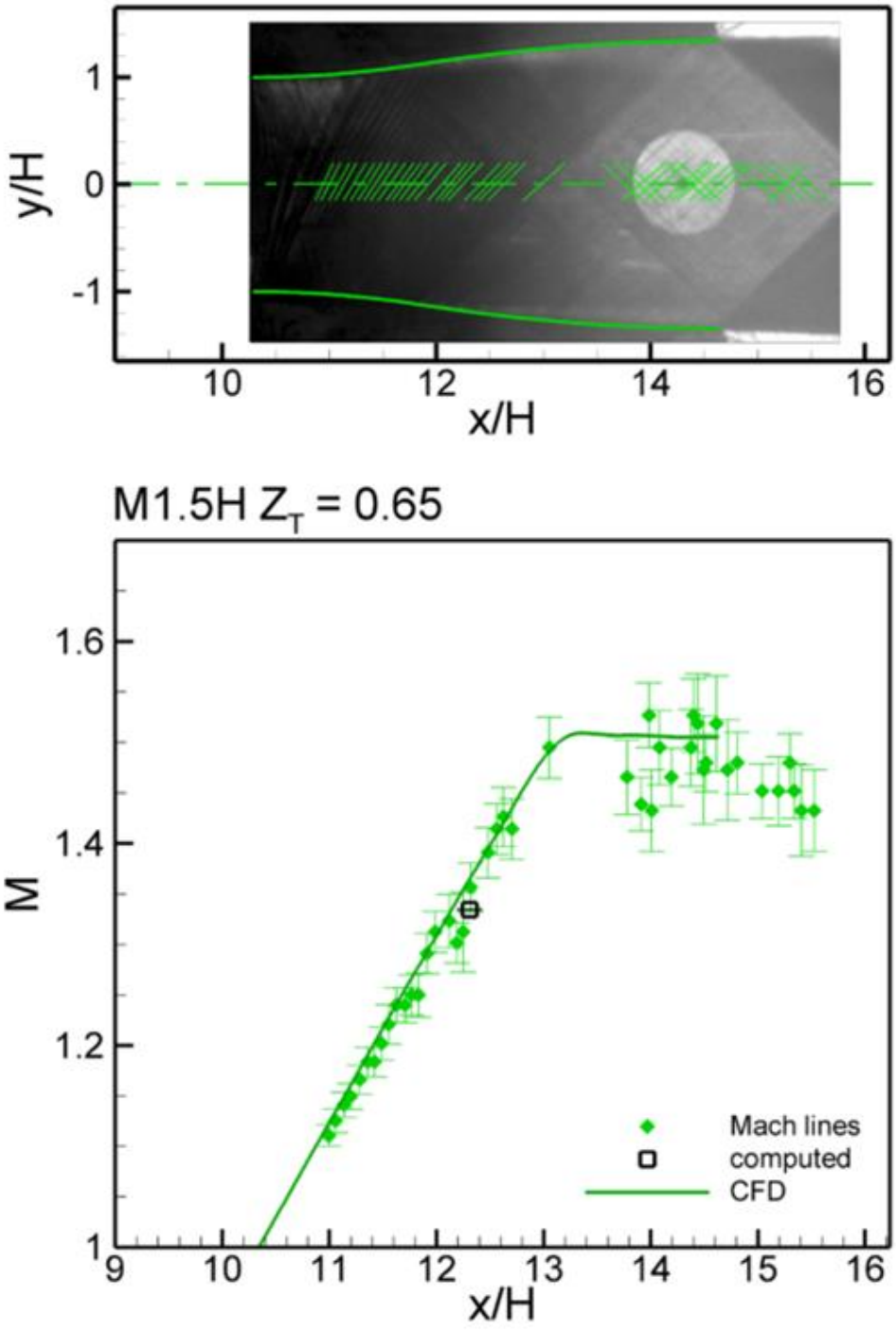

Figure 20. Schlieren image (**top**) and Mach numbers obtained from Mach lines (**bottom**) for a nozzle flow of MDM at $Z = 0.65$ (taken from [97]).

The disadvantage of the background-oriented schlieren approach is the somewhat lower resolution. In principle, achieving a higher resolution than the length scale of the background pattern is impossible. Regular and stochastic patterns can be chosen (in Figure 21, a stochastic dot pattern on the backplate of a test section was applied). It is not

helpful to reduce the length scale of the pattern up to the level where vibrations of the test rig or the optical resolution limit would be reached. In practice, the BOS approach cannot provide as sharp shock visualizations as the conventional schlieren systems. However, the advantage of visualizing even small density fluctuations and the relatively simple setup makes the BOS technique a powerful tool for compressible flow investigations. In Figure 22, the vortex street caused by the stem of a hot-wire probe downstream of a turbine cascade operated with Novec 649 at an exit Mach number of $Ma = 0.6$ is shown. The background pattern was, in this case, the natural roughness of the metal-printed cascade, and no further preparation was needed. The density gradients due to the vortex street are the dominating feature in Figure 22. That also indicates that, even in subsonic flow, the BOS approach can provide valuable insights into flow details.

Finally, the focusing schlieren system (Figure 17d) might be mentioned, because this approach is precious for local compressible flow phenomena, such as the compressible flow through a turbine tip gap [122]. The idea of a focusing schlieren approach was first described by Schardin [123] more than 70 years ago, but due to World War II, he was unable to pursue his idea further. The most recent developments to the method were made by Weinstein [124], who devised what has been termed in the literature [108] as "the modern focusing schlieren system." The high value of a focusing schlieren system for detailed investigations of three-dimensional turbine flow features was demonstrated by Passmann et al. [122], who considered the flow of air through an idealized turbine vane and a transonic cascade with tip gaps. So far, no results have been reported for applying this exciting schlieren technique to non-ideal compressible flows. Still, in the future, the use of focusing schlieren systems might also be expected in this area.

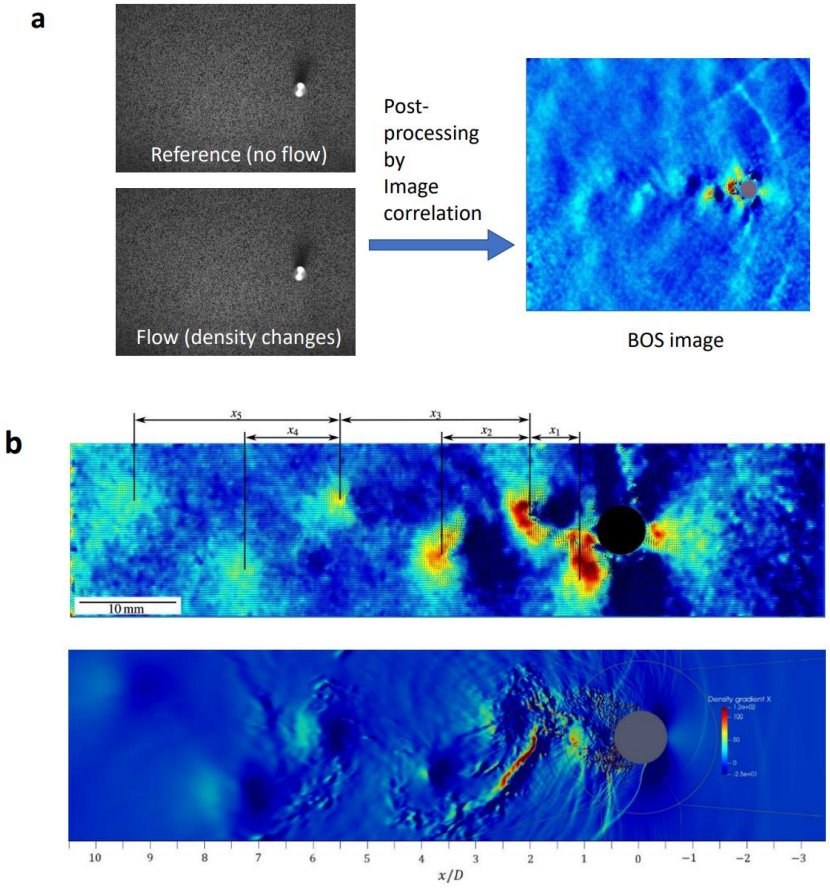

Figure 21. Principle and application of the BOS technique when applied to a circular cylinder: (**a**) schematics of the BOS working principle; (**b**) comparison of a BOS image with the instantaneous density gradient computed by LES (from [121]).

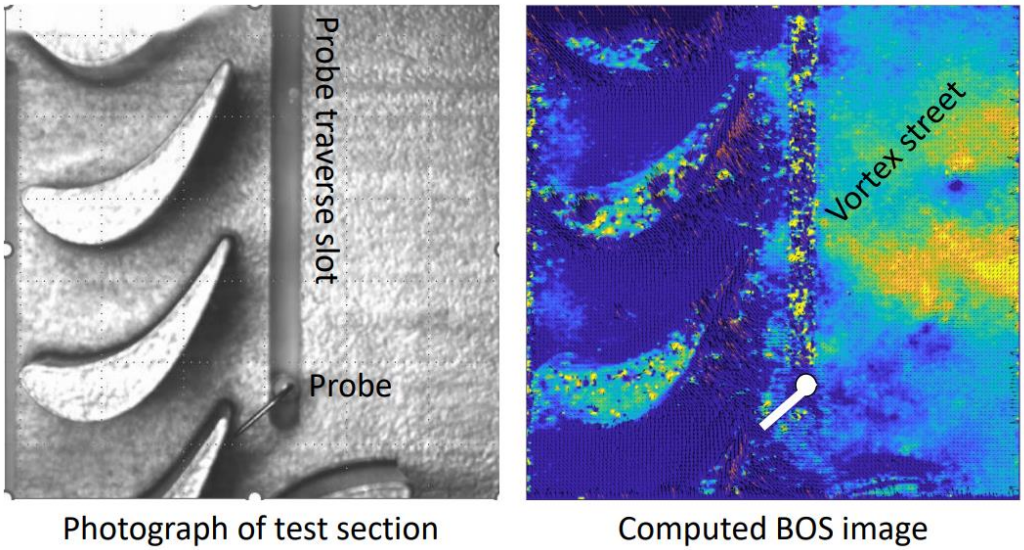

Figure 22. Background-oriented schlieren image of the flow of Novec 649 through a turbine cascade operated at an exit number of *Ma* = 0.6. The dominant feature is the vortex street in the wake of the probe stem downstream of the cascade. Pictures were taken at a test campaign at CLOWT in 2022.

5.2. Laser Doppler Velocimetry (LDV) Technique

Laser Doppler velocimetry (LDV) is a well-established experimental technique that investigates a wide range of complex flows and fluid dynamic phenomena. A comprehensive review of the principles, data analysis, and practical implementation of the LDV technique can be found in [125]. The era of LDV began in the mid-1960s after the introduction of lasers. The great advantage of LDV (and of PIV) is its non-intrusive nature. Especially in the case of high-speed flows, where solid Pitot or hot-wire probes can massively disturb the flow (see Figure 22 or Figures 14 and 15), the laser-based methods only require optical access to the measurement zone and the introduction of small particles. Conceptually, LDV enables a direct approach to determine the velocity field **w** without employing the equation of states or isentropic flow relations for the data reduction process. Hence, the experimental uncertainty level due to the uncertainties regarding the employed thermodynamic ties and the impact of error propagation might be avoided in principle.

The fundamental phenomenon behind LDV is the Doppler shift of light scattered from a small particle moving with the particle velocity w_p. Ideally, this particle velocity is identical to the fluid velocity w. In the case of microscopic particles of orders 0.1 up to 1 µm, this situation can be achieved due to the particle drag. However, suppose the velocity field is not uniform. In that case, the particle should respond quickly to the changes, and, hence, the dynamic response time of the particle must be much smaller than the characteristic time scale of the flow. That is sometimes difficult to achieve in high-speed flows or regions characterized by extraordinary changes in velocity. The application of LDV requires the introduction of small particles to the fluid under investigation. This is known as seeding. The selection of the seeding particles is vital for the success of the LDV method. The density of the particles and the fluid should be equal for ideal seeding particles to minimize dynamic effects or buoyancy issues. That requirement can hardly be realized in vapors or gases. A further trade-off problem is caused by the need to use small particles for dynamic reasons to ensure a sufficient signal-to-noise ratio (SNR) for the Doppler signal of the scattered light. The latter would be improved by increasing the particle size. In addition, high refractive index materials should be used to increase the scattering in the ambient fluid with its own refractive index. The added particles must not disturb the flow to be measured. If the LDV method should be applied to vapors at elevated temperatures (and pressure), the seeding particles should be stable enough during the measurement. In Table 4, some potential materials for seeding particles are listed. Since the density of

vapors or gases is, even at high-pressure levels, much lower than the densities listed in Table 4, no perfect seeding particle is available.

Table 4. Properties of seeding particle material.

Material	Refractive Index	Density	Melting Temperature
TiO_2	2.6 up to 2.9	3900–4200 kg/m^3	1840 °C
Al_2O_3	1.79	3960 kg/m^3	2015 °C
SiO_2	1.45	2200 kg/m^3	1710 °C
SiC	2.6	3200 kg/m^3	2700 °C

The first application of LDV for direct velocity measurements in non-ideal compressible flows was performed at the CREA laboratory of the Politecnico di Milano. The first report [106] was published in 2020, and a detailed research article [126] followed one year later. The design and the commissioning of a laser Doppler velocimetry seeding system for non-ideal fluid flows were proposed earlier in 2016 by Gallarini et al. [127]. The seeding system is crucial for NICFD applications, and no commercial or standard seeding system can be used for organic vapors at elevated temperature and pressure levels. As seeding particles, nanosized TiO_2 powder with particle dimensions of orders 150 up to 250 nm were used. To inject the particles into the vapor flow in the wind tunnel, the seeding system shown in Figure 23 was designed and used. The flow conditions for which the seeding system was designed were a maximum pressure of about 25 bar and a maximum temperature of about 300 °C in the wind tunnel. The principle of the seeding system was to employ a liquid suspension of the solid seeding particles in the working fluid, which was injected through an atomizer at high pressure and temperature in the plenum ahead of the test section of the wind tunnel. The small droplets of the injected liquid with the seeding particle suspension evaporated, thus releasing the solid particle to be entrained in the flow of the test section of the wind tunnel.

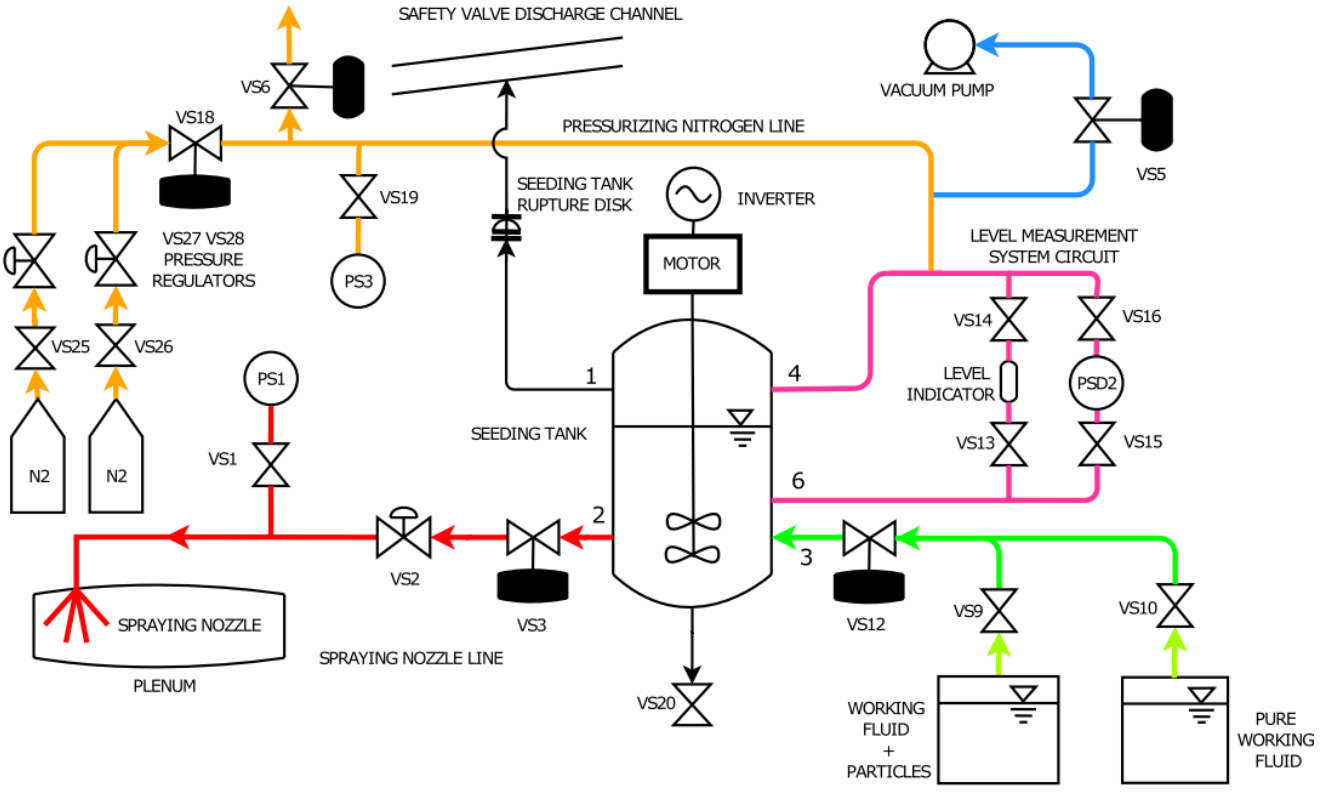

Figure 23. Seeding system for LDV application in non-ideal compressible flows (from [126]).

The LDV setup used in the study [126] was a two-component back-scattering system, which employed two 1 W diode-pumped solid-state lasers. The two laser beams each exhibited a diameter of about 1 mm and a wavelength of 489.5 nm and 513.9 nm, respectively. A 40 MHz frequency shift was applied to each couple of laser beams to avoid directional ambiguity. The burst spectrum analyzer was a Dantec F 800 component with a maximum input frequency of 200 MHz. In contrast to the seeding system, which was entirely customized, commercial laser equipment was used for LDV measurements. Details about the data processing can be found in [126].

During experiments, significant density changes can occur in the vapor. Hence, the refractive index of the vapor changed as well. This might cause changes in the laser optical paths. A discussion of the resulting uncertainty in actual LDV measurements is provided in [126].

As of the writing of this review paper, the nozzle flow experiments [126] represent the only application of LDV for non-ideal compressible flows reported in the open literature. Still, the use of this powerful tool can be expected in the future for other configurations.

5.3. Particle Image Velocimetry (PIV) Technique

The particle image velocimetry (PIV) technique was initiated in the 1980s. The fundamental principle of PIV is the calculation of the velocity of tracer particles from a sequence of photographs of the seeded and illuminated flow field. The velocity calculation is based on a correlation technique, and details about PIV can be found in [128] or [129], among other texts about flow measurement. Whereas LDV can be used to determine the velocity at a small measurement volume (i.e., the local values are obtained at a point), the PIV technique enables insights into the two- or even three-dimensional velocity field. However, in the case of high-speed flows, strict requirements on illumination and exposure time result.

The use of PIV for flows of dense gases has not been reported in the open literature so far. Probably the closest relevant examples are the use of PIV in a gas–liquid two-phase nozzle flow of CO_2 by Ueno et al. [130] and the Rayleigh–Benard convection of a supercritical fluid [131], as well as a feasibility study [107]. In this feasibility study, low-speed flows of an organic vapor (D4) were considered. It was found that the D4 vapor was sufficiently transparent to conduct PIV experiments, and evaporating the fluid with TiO2 seeding particles made it possible to obtain a proper tracer distribution. Hence, an external seeder was not needed. It was inferred in [107] that PIV is feasible in low-speed flows of hot organic vapors. Further work will be devoted to devising a seeding strategy that makes it possible to perform PIV in supersonic and transonic flows in the ORCHID test facility. Such high-speed PIV experiments are in work as of the writing of this paper, but no results have been published yet.

6. Hot-Wire Anemometry

Hot-wire anemometry (HWA) has been used as the primary tool for turbulence research. Still, it also provides relevant data for validating computational fluid dynamics (CFD methods) and their turbulence modeling capabilities. The fundamentals of hot-wire anemometry can be found in [132–136]. In incompressible flows, hot-wire anemometry has been used for a century. Later, several efforts were made to exploit this technique for compressible perfect gas flow [137–148] as well. Although three different operation modes for HWA can be distinguished, the constant temperature anemometry (CTA) approach is the most popular one.

The use of HWA for dense gases or non-ideal compressible flows is somewhat new, and the first results of measurements using Novec 649 at high subsonic flow conditions can be found in [149]. A detailed discussion of an efficient calibration was recently proposed in [150], and an application of HWA in grid-generated turbulence was shown in [151]. While the application of hot-wire anemometry is relatively straightforward for

supersonic flow, due to the negligible Mach number dependency of the sensitivity coefficients, it still poses severe difficulties for obtaining turbulence quantities in high subsonic and, especially, in transonic flows [145]. In this flow regime, determining the sensitivity coefficients and their dependence on Mach and Reynolds numbers is relatively challenging. In addition, wire breakage, vibrations, and strain gaging problems make using hot-wire probes tricky in high-speed flow regimes. Due to the relatively high density and the low speed of sound, applying hot-wire anemometry is particularly challenging for organic vapor flows. The high density of a complex organic vapor at elevated pressure leads to relatively high wire Reynolds numbers for which, in combination with noticeable Mach numbers, little is known from experiments with air or other simple gases.

6.1. Calibration and Behavior of Sensitivity Coefficients

To employ the hot-wire technique, the entire system must be calibrated. Since even small changes can result in noticeable deviations, the calibration should be conducted under conditions identical to the application conditions. As in the case of Pitot probes, which contrast the perfect gas case, in non-ideal flows, directional probes require a calibration procedure that is both fluid-specific and thermodynamic condition-specific. An illustration of a calibration section from the CLOWT test facility is shown in Figure 24.

The static and total pressures were measured directly in the calibration section through wall taps and a miniaturized Pitot probe that was close to the rotatable mounted hot-wire probe (CTA). The closed-loop wind tunnel at CLOWT, see Section 3, could effectively be used for calibrating hot-wire probes due to its ability to control the total temperature and pressure level. Furthermore, its background turbulence level is relatively low (of orders 0.2% up to 0.6%, which were obtained by hot-wire anemometry in the empty test section). The actual flow rate can be determined independently by a mass flux sensor in the return of the wind tunnel. Since steady-state operation with negligible temperature and pressure drifts can be set, a complete calibration, including determination of the angle sensitivity due to different probe orientations to the flow, is possible. However, in closed calibration sections, as are shown in Figure 24, only high subsonic flow conditions are achievable, due to the choking effect and the blockage of the probes. The probes must be mounted downstream of a nozzle or an open jet configuration within the test facility for transonic or supersonic flow conditions. The uncertainty analysis for calibration can, in principle, follow the approach recommended in [152,153].

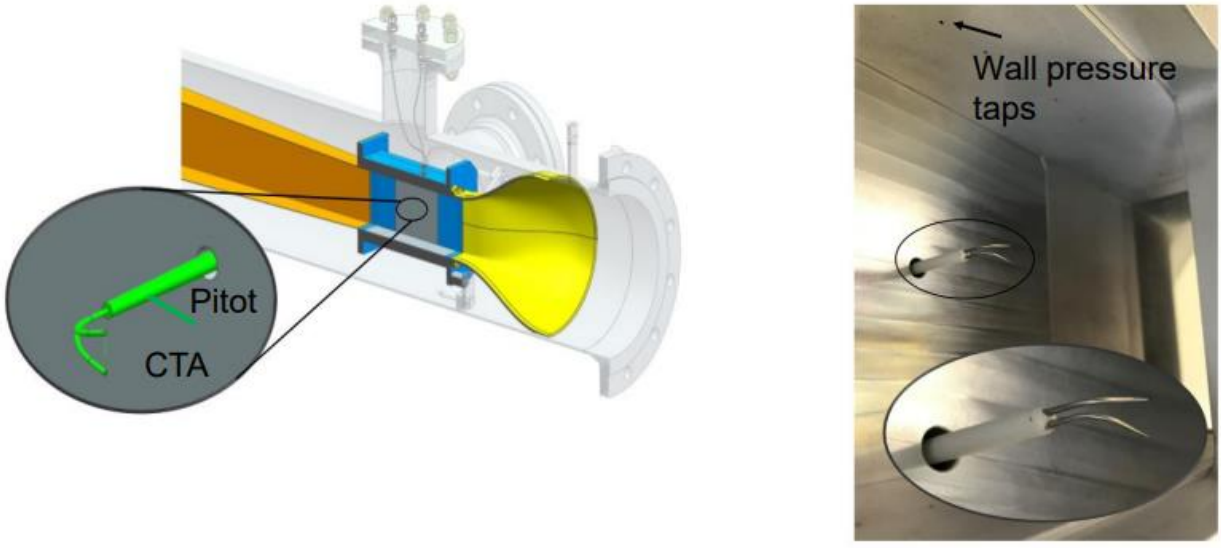

Figure 24. Closed calibration section for hot-wire probes under non-ideal compressible flow conditions.

A full calibration of a CTA probe requires several tests, and it is not ensured that the probes will survive the calibration process. Due to the high dynamic loads, some probes will break after a few minutes of operation in heavy organic vapors, while others can be used for more than eight hours. In any case, it is desirable to have the capability to repair and produce probes in the laboratory.

The starting point for the calibration is the selection of an appropriate heat transfer correlation. Following de Souza and Tavoularis [147], a modified King correlation

$$E^2 = A(Ma, T_o) + B(Ma, T_o)(\rho U)^n \tag{22}$$

for a fixed wire overheat ratio τ and total fluid temperature T_o has proven its reliability for organic vapors [150]. The exponent n can often be set to n = ½. In CTA systems, the electrical output signal (voltage) E^2 can be identified with the Nusselt number (with an appropriate proportionality constant as a trivial multiplier). A linearization of the heat transfer equation and the use of logarithmic derivatives yield the sensitivity coefficients

$$S_u = \left(\frac{\partial \ln E}{\partial \ln U}\right)_{\rho,T_o},\ S_\rho = \left(\frac{\partial \ln E}{\partial \ln \rho}\right)_{U,T_o} \text{ and } S_T = \left(\frac{\partial \ln E}{\partial \ln T_o}\right)_{\rho,U} \tag{23}$$

for relating the voltage signal fluctuation to the velocity, density, and total temperature fluctuations, which are defined as:

$$\frac{E'}{\bar{E}} = S_u \frac{U'}{\bar{U}} + S_\rho \frac{\rho'}{\bar{\rho}} + S_T \frac{T_o'}{\bar{T}_o'} \tag{24}$$

For supersonic flow (Ma > 1.2), Morkovin [139] has shown that the Mach number influence for the sensitivity coefficients is small and may be ignored. Therefore, the sensitivity coefficients for density and velocity become equal, and, formally, a simplified relation

$$\frac{E'}{\bar{E}} = S_{\rho u} \frac{(\rho U)'}{\overline{(\rho U)}} + S_T \frac{T'_o}{\bar{T}'_o} \tag{25}$$

results. The equality of the two sensitivity coefficients for density and velocity significantly reduces the data reduction and calibration efforts when measuring turbulent fluctuations quantities. Still, their equality must be proven individually for each hot-wire anemometer and flow situation. Interestingly, the relatively high wire Reynolds numbers for organic vapors support this simplification, as has been demonstrated in [150].

6.2. Application and Operational Issues

The application of HWA and its correct data interpretation sometimes require special attention. In addition to the general considerations for using HWA, the following special operation issues related to measurements in flows of heavy compressible vapors are discussed.

The high density of the organic vapor leads to relatively high wire and grid Reynolds numbers. Due to the resulting small Kolmogorov scale η, corrections were needed to account for the systematic attenuation of high-frequency signals by probes with finite wire lengths l. That issue is absent in the case of a static calibration using a wind tunnel with low background turbulence, as was described in the previous subsection. However, suitable correction schemes should be considered in actual measurements, as has been explained in [154,155]. This was pointed out in [156], and it was shown that the classical correction scheme, due to the work of Wyngaard [155] that was initially developed for isotropic turbulence in incompressible flows, is still applicable for the high subsonic flow of an organic vapor. Corresponding correction formulas can be established by using hot-wire probes with different lengths and their extrapolation to a probe with a vanishing length [154]. In the study [156], two probes with the same electrical resistance but different wire lengths and diameters (l = 4 mm (d = 10 μm) and l = 1 mm (d = 5 μm)) were used.

Although Wyngaard's correction scheme is only theoretically justified for isotropic turbulence, no better alternative seems to be available yet.

Somewhat related to the small turbulent length scales in high-speed flows of organic vapors is the high cut-off frequency of the employed electrical bridge and amplifier (i.e., the anemometer circuit). Cut-off frequencies of more than 100 kHz are not uncommon for transonic or supersonic organic vapor flows. This fact makes alternative concepts, like the constant voltage anemometer [157] or the atomic layer thermo-pile ALTP sensor [158], interesting for future experiments.

In addition to the strong flow disturbances caused by the probes, as are demonstrated by the vortex street downstream of the stem that is shown in Figure 22, the high dynamic loads in high-speed flows of dense gases can create severe vibration issues. Observing the probe in the test section through a high-speed camera makes it possible to determine whether serious vibration issues exist. For instance, this was done for the arrangement shown in Figure 22, and indeed two vibrations were observed for the probe subjected to a stream of Novec 649 at 2 bar and 100 °C at an exit Mach number of $Ma = 0.64$. The structural analysis leads to the prediction that the typical natural frequencies of specific HWA probe devices, including a stem, are of the order of 1 kHz.

The importance of accounting for the different operational issues for a correct data interpretation can be illustrated by an example. Figure 25 shows the HWA signal (power spectrum) downstream of the trailing edge of a turbine cascade (corresponding to the setup already shown in Figure 22). In the spectrum shown in Figure 25, the compressor running speed and its blade passing frequencies can be detected even after passing the settling chamber, turbulence screens, and the turbine cascade. This demonstrates that HWA is a very sensitive flow measurement technique. The two mechanical vibration frequencies of the probe contribute to the spectrum as well. The vortex shedding frequency due to the probe stem corresponded to a Strouhal number of $St_{stem} = 0.17–0.20$, which is in reasonable agreement with the literature data for a cylinder subjected to a constant stream [159]. The trailing edge vortex shedding Strouhal number was found to be $St = 0.24 \pm 0.2$, which was in excellent agreement with the values reported in [159,160] for that turbine cascade. The fact that two vortex shedding responses (denoted by 1x and 2x in Figure 25) occurred in the CTA spectrum was because the HWA was insensitive to the flow direction [134].

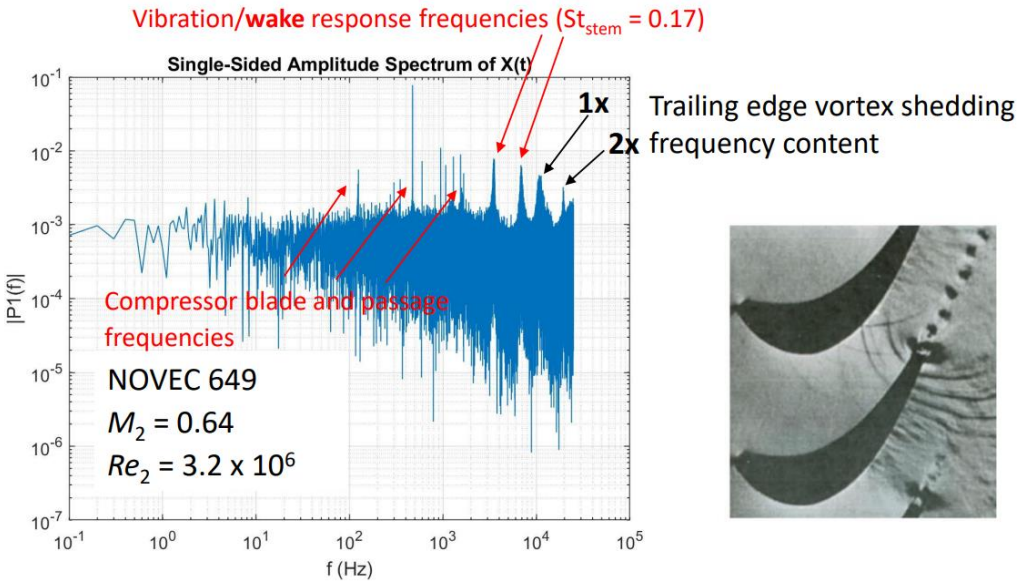

Figure 25. Power spectrum of a CTA probe placed downstream of a turbine cascade (see Figure 22), including a break-down of the frequency content.

7. Concluding Remarks

Whereas the theoretical study of non-ideal compressible fluid dynamics (NICFD) has a long tradition, the systematic experimental investigation of it is a relatively young discipline. Based on established flow measurement techniques, several research groups have developed pneumatic, optical, and thermal techniques that are well-suited for NICFD. The application of these experimental methods has allowed exciting insights into the aerodynamics and thermodynamics of non-ideal compressible flows.

It can be expected that the development and the utilization of flow measurements techniques will be continued. For instance, the use of multi-hole probes or high-speed PIV applications have not been published in the open literature so far. Hence, measurement techniques for NICFD are a research area which is anything but finished.

Currently, the impact of real gas behavior on the dimensional analysis is not fully understood. Therefore, more detailed measurements are required to establish the right set of similarity numbers for the design of components and flow devices that are subjected to non-ideal compressible flows.

In addition to testing the theory, NICFD flow measurement techniques provide data sets which are needed for validating computational fluid dynamics (CFD) methods. Since numerical loss predictions for turbomachinery are notoriously uncertain, there will be a need for detailed flow and loss measurements for turbine cascades working with organic vapors. In combination with reliable numerical methods, this research will enable the design of more efficient turbines for ORC power systems.

Funding: The preparation of this review paper received no external funding except for the financial support of the DFG (Grant Number: Wi 1840) regarding research about measurement techniques and application for ORC turbines (under the project title "REGAL-ORC"), which is highly acknowledged by the author.

Institutional Review Board Statement: Not applicable.

Informed Consent Statement: Not applicable.

Data Availability Statement: Not applicable.

Acknowledgments: The author of this review paper had the luck of having many discussions with outstanding experts about the topic of this contribution for many years. Among the numerous colleagues and their contributions, the author would like to acknowledge the precious suggestions by Andrea Spinelli, Milano, Andrew Wheeler, Cambridge, and Adam Head at Delft. Without the extraordinary efforts of the CLOWT team members during many years of research at the Muenster University of Applied Sciences, the author of this paper would hardly be in a position to review measurement techniques for NICFD. Thus, special thanks are expressed to Felix Reinker, Max Passmann (now in Ruhr-Universität Bochum, Germany), Leander Hake, Stephan Sundermeier, and to several other supporters of the CLOWT. Finally, the author would like to express his thanks to the editor of this journal, Marcello Manna, who significantly supported this review initiative.

Conflicts of Interest: The author declares no conflict of interest.

Nomenclature

A	heat transfer correlation coefficient, V^2
a	speed of sound, m/s
B	heat transfer correlation coefficient
c	velocity, m/s
c_p	isobaric specific heat, J/(kg K)
c_v	isochoric specific heat, J/(kg K)
E	electrical voltage, V
f	function, -
$\mathbf{f}$	body force, m/s^2
h	specific enthalpy, J/kg
l	length, m
Ma	Mach number, -

p	pressure, Pa
Pr	Prandtl number, -
R	specific gas constant, J/(kg K)
Re	Reynolds number, -
S	sensitivity coefficient, -
$\mathbf{S}$	stress tensor, Pa/m
s	specific entropy, J/(kg K)
St	Strouhal number, -
T	temperature, K
t	time, s
U	velocity, m/s
v	specific volume, m^3/kg
$\mathbf{w}$	velocity vector, m/s
Z	compressibility factor, -
Greek symbols	
α	angle, °
Γ	fundamental derivative, -
γ	isentropic exponent, -
ρ	density, kg/m^3
λ	thermal conductivity, W/(m K)
μ	dynamic viscosity, Pa s
η	Kolmogorov length scale, m
η	efficiency, -
$\mathbf{\Phi}$	viscous dissipation, Pa^2
ϕ	flow coefficient, -
Subscripts	
c	critical point
o	total or stagnation condition
1	inflow or upstream of Pitot probe
2	exit or downstream of Pitot probe shock
Superscript	
‘	fluctuating part

References

1. Colonna, P.; Casati, E.; Trapp, C.; Mathijssen, T.; Larjola, J.; Turunen-Saaresti, T.; Uusitalo, A. Organic Rankine cycle power systems: From the concept to current technology, applications, and an outlook to the future. *ASME J. Eng. Gas Turb. Power* **2015**, *137*, 100801.
2. Macchi, E.; Astolfi, M., Eds. *Organic Rankine Cycle (ORC) Power Systems: Technologies and Applications*; Woodhead Publishing: Cambridge, UK, 2016.
3. White, M.T.; Bianchi, G.; Chai, L.; Tassou, S.A.; Sayma, A.I. Review of supercritical CO_2 technologies and systems for power generation. *Appl. Therm. Eng.* **2021**, *185*, 116447.
4. Kluwick, A. *Nonlinear Waves in Real Fluids*; Springer: Wien, Austria, 1991.
5. Kluwick, A. Handbook of shockwaves. In *Theory of Shock Waves: Rarefaction Shocks*; Academic Press: Cambridge, MA, USA, 2001; Volume 1, pp. 339–411.
6. Kluwick, A. Shock discontinuities: From classical to non-classical shocks. *Acta Mech.* **2018**, *229*, 515–533.
7. Reynolds, W.C.; Colonna, P. *Thermodynamics: Fundamentals and Engineering Applications*; Cambridge University Press: Cambridge, UK, 2018.
8. Guardone, A.; Colonna, P.; Wheeler, A., Eds. 1st international seminar on non-ideal compressible fluid dynamics for propulsion and power. *J. Physics Conf. Ser.* **2017**, *821*, 011001.
9. Duhem, P. On the propagation of shock waves in fluids. *Z. Phys. Chem.* **1909**, *69*, 169–186.
10. Becker, R. Stoßwelle und Detonation. *Z. Für Phys.* **1922**, *8*, 321–362.
11. Bethe, H.A. *The Theory of Shock Waves for an Arbitrary Equation of State*; Report No. 545; Office of Scientific Research and Development: Washington, DC, USA, 1942.
12. Zel’dovich, Y.B. On the possibility of rarefaction shock waves. *Zh. Eksp. Teor. Fiz.* **1946**, *4*, 363–364.
13. Thompson, P.A. A Fundamental Derivative in Gas Dynamics. *Phys. Fluids* **1971**, *14*, 1843–1849.
14. Anderson, W.K. Numerical Study on Using Sulfur Hexafluoride as a Wind Tunnel Test Gas. *AIAA J.* **1991**, *29*, 2179–2180.
15. Anders, J.B. Heavy Gas Wind Tunnel Research at Langley Research Center. ASME Paper. In Proceedings of the Fluids Engineering Conference, Washington, DC, USA, 20–24 June 1993; sponsored by the Fluids Engineering Division, 93-FE-5.

16. Anders, J.B.; Anderson, W.K.; Murthy, A.V. The Use of Heavy Gas for Increased Reynolds Numbers in Transonic Wind Tunnels. In Proceedings of the 20th AIAA Advanced Measurement and Ground Testing Technology Conference, Albuquerque, NM, USA, 15–18 June 1998; AIAA-98-2882.
17. Rist, D. *Dynamik Realer Gase*; Springer: Berlin, Germany, 1996.
18. Boncinelli, P.; Rubechini, F.; Arnone, A.; Cecconi, M.; Cortese, C. Real gas effects in turbomachinery flows: A computational fluid dynamics model for fast computations. *ASME J. Turbomach.* **2004**, *126*, 268–276.
19. Brun, K.; Friedman, P.; Dennis, R., Eds. *Fundamentals and Application of Supercritical Carbon Dioxide Based Power Cycles*; Woodhead Publishing: Sawston/Cambridge, UK, 2017.
20. Head, A.J. Novel Experiments for the Investigation of Non-Ideal Compressible Fluid Dynamics: The ORCHID and First Results of Optical Measurements. Ph.D. Thesis, TU Delft, Delft, The Netherlands, 2021.
21. Landau, L.D. On shock waves. *J. Phys. USSR* **1942**, *6*, 229–230.
22. Hayes, W.D. The basic theory of gasdynamic discontinuities. In *Fundamentals of Gasdynamics*; Princeton University Press: Princeton, NJ, USA, 1958; Volume 2.
23. Vimercati, D.; Gori, G.; Spinelli, A.; Guardone, A. Non-Ideal Effects on the Typical Trailing Edge Shock Pattern of Orc Turbine Blades. *Energy Procedia* **2017**, *129*, 1109–1116.
24. Colonna, P.; Nannan, N.R.; Guardone, A.; van der Stelt, T.P. On the computation of the fundamental derivative of gas dynamics using equation of states. *Fluid Phase Equilibria* **2009**, *286*, 43–54.
25. Morren, S.H. *Transonic Aerodynamics of Dense Gases*; NASA TM-103722; Lewis Research Center: Cleveland, OH, USA, 1991.
26. Lemmon, E.W.; Huber, M.L.; McLinden, M.O. *NIST Reference Database 23: Reference Fluid Thermodynamic and Transport Properties–REFPROP, Version 9.1*; Standard Reference Data Program: Gaithersburg, MD, USA, 2013.
27. Traupel, W. Zur Dynamik realer Gase. *Forsch. Ing*. **1952**, *18*, 3–9.
28. Traupel, W. *Thermische Turbomaschinen—Erster Band*, 2nd ed.; Springer: Berlin, Germany, 1966; Chapter 1.
29. Kouremenos, D.A.; Antonopoulos, K.A. Isentropic Exponents of Real Gases and Application for the Air at Temperatures from 150 K to 450 K. *Acta Mech.* **1986**, *65*, 81–99.
30. aus der Wiesche, S.; Reinker, F. Dimensional analysis and performance laws for organic vapor flow turbomachinery. *Energy* **2022**, *257*, 124635.
31. Taylor, E.S. *Dimensional Analysis for Engineers*; Clarendon: Oxford, UK, 1974.
32. Dejc, M.E.; Trojanovskij, B.M. *Untersuchung und Berechnung Axialer Turbinenstufen*; VEB Verlag Technik: Berlin, Germany, 1973.
33. Turunen-Saaresti, T.; Uusitalo, A.; Honkatukia, J. Design and testing of high temperature micro-ORC test stand using Siloxane as working fluid. In *Journal of Physics: Conference Series*; IOP Publishing: Bristol, UK, 2017; Volume 821, p. 012024.
34. Seume, J.R.; Peters, M.; Kunte, H. Design and test of a 10kW ORC supersonic turbine generator. In *Journal of Physics: Conference Series*; IOP Publishing: Bristol, UK, 2017; Volume 821, p. 012023.
35. Park, B.S.; Usman, M.; Imran, M.; Pesyridis, A. Review of Organic Rankine Cycle experimental data trends. *Energy Convers. Manag.* **2018**, *173*, 679–691.
36. Spinelli, A.; Guardone, A.; De Servi, C.; Colonna, P.; Reinker, F.; aus der Wiesche, S.; Robertson, M.; Martinez-Botas, R.F. Experimental facilities for non-ideal compressible vapour flows. *ERCOFTAC Bull.* **2020**, *124*, 59–66.
37. Bradley, J. *Shock Waves in Chemistry and Physics*; Chapman and Hall: London, UK, 1962.
38. Gaydon, A.G.; Hurle, I.R. *The Shock Tube in High Temperature Chemical Physics*; Chapman and Hall: London, UK, 1963.
39. Soloukhin, R.I. *Shock Waves and Detonations in Gases*; Mono Books: Baltimore, MD, USA, 1966.
40. Baumgärtner, D.; Otter, J.J.; Wheeler, A.P. The Effect of Isentropic Exponent on Transonic Turbine Performance. *ASME J. Turbomach.* **2020**, *142*, 081007. https://doi.org/10.1115/1.4046528.
41. Dura Galiana, F.J.; Wheeler, A.P.; Ong, J. A Study of trailing-edge losses in organic Rankine cycle turbines. In Proceedings of the ASME Turbo Expo 2015: Turbine Technical Conference and Exposition, Montreal, QC, Canada, 15–19 June 2015; GT2015-42920, V02AT38A020, 12p.
42. Fergason, S.H.; Guardone, A.; Argrow, B.M. Construction and Validation of a Dense Gas Shock Tube. *J. Thermophys. Heat Transf.* **2003**, *17*, 326–333.
43. Colonna, P.; Guardone, A.; Nannan, N.R.; Zamfirescu, C. Design of the dense gas flexible asymmetric shock tube. *ASME J. Fluids Eng.* **2008**, *130*, 034501.
44. Mathijssen, T.; Gallo, M.; Casati, E.; Nannan, N.R.; Zamfirescu, C.; Guardone, A.; Colonna, P. The Flexible Asymmetric Shock Tube (FAST): A Ludwieg tube facility for wave propagation measurements in high-temperature vapours of organic fluids. *Exp. Fluids* **2015**, *56*, 195.
45. Chandrasekaran, N.B.; Michelis, T.; Mercier, B.; Colonna, P. Preliminary experiments in high temperature vapours of organic fluids in the Asymmetric Shock Tube for Experiments on Rarefaction Waves (ASTER). In Proceedings of the 4th International Seminar on Non-Ideal Compressible Fluid Dynamics (NICFD2022), City University, London, UK, 3–4 November 2022.
46. Dettleff, G.; Thompson, P.A.; Meier, E.A.; Speckmann, H. An experimental study of liquefaction shock waves. *J. Fluid Mech.* **1979**, *95*, 279–304.
47. Dettleff, G.; Thompson, P.A.; Meier, E.A. Initial experimental results for liquefaction shock waves in organic fluids. *Arch. Mech.* **1976**, *28*, 827–836.
48. Duff, K. Non-Equilibrium Condensation of Carbon Dioxide in Supersonic Nozzles. Ph.D. Thesis, M.I.T., Cambridge, MA, USA, 1966.

49. Lettieri, C.; Yang, D.; Spakoszky, Z. An investigation of condensation effects in supercritical carbon dioxide compressors. *ASME J. Eng. Gas Turbine Power* **2015**, *137*, 082602.
50. Spinelli, A.; Dossena, V.; Gaetani, P.; Osnaghi, C.; Colombo, D. Design of a Test Rig for Organic Vapours. In Proceedings of the ASME Turbo Expo 2010, Glasgow, UK, 14–18 June 2010.
51. Spinelli, A.; Dossena, V.; Gaetani, P.P.; Casella, F. Design, Simulation, and Construction of a Test Rig for Organic Vapors. *ASME J. Eng. Gas Turb. Power* **2013**, *135*, 10.
52. Spinelli, A.; Guardone, A.; Cozzi, F.; Cammi, G.; Cheli, R.; Zocca, M.; Gaetani, P.; Dossena, V. Experimental Observation of Non-ideal Nozzle Flow of Siloxane Vapor MDM. In Proceedings of the 3rd International Seminar on ORC Power Systems, Brussels, Belgium, 12–14 October 2015.
53. Spinelli, A.; Cozzi, F.; Cammi, G.; Zocca, M.; Gaetani, P.; Dossena, V.; Guardone, A. Preliminary characterization of an expanding flow of siloxane vapor MDM. In *Journal of Physics: Conference Series*; IOP Publishing: Bristol, UK, 2017; Volume 821, p. 012022.
54. Spinelli, A.; Cammi, G.; Conti, C.C.; Gallarini, S.; Zocca, M.; Cozzi, F.; Gaetani, P.; Dossena, V.; Guardone, A. Experimental observation and thermodynamic modeling of non-ideal expanding flows of siloxane MDM vapor for ORC applications. *Energy* **2019**, *168*, 285–294.
55. Robertson, M.C.; Newton, P.J.; Chen, T.; Martinez-Botas, R.F. Development and commissioning of a blowdown facility for dense gas vapours. In Proceedings of the ASME Turbo Expo 2019, Phoenix, AZ, USA, 17–21 June 2019; GT2019-91609.
56. Robertson, M.C.; Newton, P.J.; Chen, T.; Costall, A.; Martinez-Botas, R.F. Experimental and numerical study of supersonic non-ideal flows for organic Rankine cycle applications. *ASME J. Eng. Gas Turbines Power* **2020**, *142*, 081007.
57. Dixon, S.L.; Hall, C.A. *Fluid Mechanics and Thermodynamics of Turbomachinery*, 6th ed.; Butterworth-Heinemann: Burlington, MA, USA, 2010.
58. Hirsch, C., Ed. *Advanced Methods for Cascade Testing*; NATO, AGARDograph 328; Specialised Printing Services Limited: Loughton, UK, 1993; ISBN 92-835-0717-7.
59. Sieverding, C.H. Aerodynamic development of axial turbomachinery blading. In *Thermodynamics and Fluid Mechanics of Turbomachinery*; Ücer, A.S.; Stow, P.; Hirsch, C., Eds.; NATO ASI Series: Dordrecht, The Netherlands, 1985; Volume 1.
60. Reinker, F.; Hasselmann, K.; aus der Wiesche, S.; Kenig, E.Y. Thermodynamics and fluid mechanics of a closed blade cascade wind tunnel for organic vapors. *ASME J. Eng. Gas Turbine Power* **2015**, *138*, 052601.
61. Reinker, F.; Kenig, E.Y.; Passmann, M.; aus der Wiesche, S. Closed loop organic wind tunnel (CLOWT): Design, components and control system. In Proceedings of the ORC2017—4th International Seminar on ORC Power Systems, Milan, Italy, 13–15 September 2017, pp. 200–207.
62. Reinker, F.; Kenig, E.Y.; aus der Wiesche, S. CLOWT: A multifunctional test facility for the investigation of organic vapor flows. In Proceedings of the ASME 2018 5th Joint US-European Fluids Engineering Summer Conference, Montreal, QC, Canada, 15–20 June 2018.
63. Reinker, F.; Kenig, E.Y.; aus der Wiesche, S. Closed loop organic vapor wind tunnel (CLOWT: Commissioning and operational experience. In Proceedings of the ORC2019—5th International Seminar on ORC Power Systems, Athens, Greece, 9–11 September 2019.
64. Hake, L.; Reinker, F.; Wagner, R.; aus der Wiesche, S.; Schatz, M. The Profile Loss of Additive Manufactured Blades for Organic Rankine Cycle Turbines. *Int. J. Turbomach. Propuls. Power* **2022**, *7*, 11. https://doi.org/10.3390/ijtpp7010011.
65. White, M.T.; Sayma, A.I. Design of a closed-loop optical access supersonic test facility for organic vapors. In Proceedings of the ASME Turbo Expo 2018, Oslo, Norway, June 11–15 2018; GT2018-75301.
66. Bier, K.; Ehrler, F.; Hartz, U.; Kissau, G. Zur Berechnung von Düsenströmungen stark realer Gase. *Forsch. Lng. Wes.* **1977**, *43*, 175–184.
67. Head, A.; De Servi, C.; Casati, E.; Pini, M.; Colonna, P. Preliminary design of the ORCHID: A facility for studying non-ideal compressible fluid dynamics and testing ORC expanders. In Proceedings of ASME Turbo Expo 2016, Seoul, South Korea, 13–17 June 2016; GT2016-56103.
68. Beltrame, F.; Head, A.J.; De Servi, C.; Pini, M.; Schrijer, F.; Colonna, P. First Experiments and Commissioning of the ORCHID Nozzle Test Section. In *NICFD 2020: Proceedings of the 3rd International Seminar on Non-Ideal Compressible Fluid Dynamics for Propulsion*; Pini, M. Ed.; ERCOFTAC Series; Springer: Berlin/Heidelberg, Germany, 2021; Volume 28, pp. 169–178. https://doi.org/10.1007/978-3-030-69306-0_18.
69. White, M. Workshop on experimental test facilities. In Proceedings of the 4th International Seminar on Non-Ideal Compressible Fluid Dynamics (NICFD2022), City University, London, UK, 3–4 November 2022, 2022.
70. Bradshaw, P. *Experimental Fluid Mechanics*; Pergamon Press: Oxford, UK, 1970.
71. Bradshaw, P. *An Introduction to Turbulence and Its Measurement*; Pergamon Press: Oxford, UK, 1971.
72. Eckelmann, H. *Einführung in Die Strömungsmeßtechnik*; Teubner: Stuttgart, Germany, 1997.
73. Nitsche, W.; Brunn, A. *Strömungsmesstechnik*; Springer-VDI: Berlin, Germany, 2006.
74. Tropea, C.; Yarin, A.L.; Foss, J.F., Eds. *Springer Handbook of Experimental Fluid Mechanics*; Springer: Berlin, Germany, 2007.
75. Han, J.-C.; Wright, L. *Experimental Methods in Heat Transfer and Fluid Mechanics*; CRC Press: Boca Raton, FL, USA, 2022.
76. Liepmann, H.W.; Roshko, A. *Elements of Gasdynamics*; John Wiley & Sons: New York, NY, USA, 1957.
77. John, J.E.; Keith, T.G. *Gas Dynamics*, 3rd ed.; Pearson: Upper Saddle River, NJ, USA, 2006.
78. Folsom, R.G. Review of Pitot Tubes. *Trans. Am. Soc. Mech. Eng.* **1956**, *78*, 1447–1460.

79. Moore, M.J.; Sieverding, C.H. *Two-Phase Steam Flow in Turbines and Separators: Theory, Instrumentation, Engineering*; Hemisphere Publishing: Washington, DC, USA,1976; Volume 1.
80. Murthy, S.; Leonard, M.; Ehresman, C. A Stagnation Pressure Probe for Droplet-Laden Air Flow. *J. Propuls.* **1986**, *2*, 195–196.
81. Harbeck, J.; Geist, S.; Schatz, M. An approach to measure total-head in wakes and near end walls at high fogging conditions. In Proceedings of the ASME Turbo Expo 2021, Virtual, 7–11 June 2021; GT2021-59190.
82. Conti, C.; Fusetti, A.; Spinelli, A.; Guardone, A. Shock losses and Pitot tube measurements in non-ideal supersonic and subsonic flows of organic vapors. In Proceedings of the 6th International Seminar on ORC Power Systems, Munich, Germany, 11–13 October 2021; p. 81.
83. Conti, C.; Fusetti, A.; Spinelli, A.; Gaetani, P.; Guardone, A. Pneumatic system for pressure probe measurements in transient flows of non-ideal vapors subject to line condensation. *Measurement* **2022**, *192*, 110802.
84. Conti, C.; Fusetti, A.; Spinelli, A.; Guardone, A. Shock loss measurements in non-ideal supersonic flows of organic vapors. *Exp. Fluids* **2022**, *63*, 117.
85. Reinker, F.; Wagner, R.; Passmann, M.; Hake, L.; aus der Wiesche, S. Performance of a rotatable cylinder pitot probe in high subsonic non-ideal gas flows. In *NICFD 2020, ERCOFTAC Series 28*; Pini, M., de Servi, C., Spinelli, A., di Mare, F., Guardone, A., Eds.; Springer International Publishing: Cham, Switzerland, 2021; pp. 144–152. https://doi.org/10.1007/978-3-030-69306-0_15.
86. aus der Wiesche, S.; Reinker, F.; Wagner, R.; Hake, L.; Passmann, M. Critical and choking Mach numbers for organic vapor flows through turbine cascades. In Proceedings of the ASME Turbo Expo 2021, Virtual, 7–11 June 2021; GT2021-59013.
87. Dura Galiana, F.J.; Wheeler, A.P.; Ong, J. A Study of trailing-edge losses in organic Rankine cycle turbines. *Proc. ASME J. Turbomach.* **2016**, *138*, 121003.
88. Reinker, F.; Wagner, R.; Hake, L.; aus der Wiesche, S. High subsonic flow of an organic vapor past a circular cylinder. *Exp. Fluids* **2021**, *62*, 54.
89. Manfredi, M.; Persico, G.; Spinelli, A.; Gaetani, P.; Dossena, V. Loss measurement strategy in ORC supersonic blade cascades. In Proceedings of the 4th International Seminar on Non-Ideal Compressible Fluid Dynamics (NICFD2022), City University, London, UK, 3–4 November 2022.
90. Manfredi, M.; Spinelli, A.; Persico, G.; Gaetani, P.; Dossena, V. Nitrogen experiments on a supersonic linear cascade for ORC applications. In Proceedings of the XXVI Biennial Symposium on Measuring Techniques in Turbomachinery, Pisa, Italy, 28–30 September 2022.
91. Baumgärtner, D. Real Gas Effects in ORC Turbines. Ph.D. Thesis, University of Cambridge, Cambridge, UK, 2020. https://doi.org/10.17863/CAM.69867.
92. Wyler, J.S. Probe Blockage Effects in Free Jets and Closed Tunnels. *ASME J. Eng. Power* **1975**, *97*, 509–514.
93. Truckenmüller, F.; Renner, M.; Stetter, H.; Hosenfeld, H. Transonic probe blockage effects in a calibration wind-tunnel and stator blade passage. In Proceedings of the ASME Turbo Expo 1996, Birmingham, UK, 10–13 June 1996; pp. 96;01–397.
94. Langford, R.W.; Keeley, K.R.; Wood, N.B. Investigation of the Transonic Calibration Characteristics of Turbine Static Pressure Probes, In Proceedings of the ASME 1982 International Gas Turbine Conference and Exhibit, London, UK, 18–22 April 1982; ASME-Paper, No. 82-GT-280.
95. Squire, L.C. Effects of Probe Supports on Measurements in Steam Turbines. In Proceedings of the ASME 1986 International Gas Turbine Conference and Exhibit, Dusseldorf, Germany, 8–12 June 1986; ASME-Paper, No. 86-GT-213.
96. Ducruet, C. A Method for Correcting Wall Pressure Measurements in Subsonic Compressible Flow. *ASME J. Fluids Eng*. **1991**, *113*, 256–260.
97. Spinelli, A.; Cammi, G.; Gallarini, S.; Zocca, M.; Cozzi, F.; Gaetani, P.; Dossena, V.; Guardone, A. Experimental evidence of non-ideal compressible effects in expanding flow of a high molecular complexity vapor. *Exp. Fluids* **2018**, *59*, 126.
98. Schollmeier, J.-N.; aus der Wiesche, S. A user-friendly pitot probe data reduction routine for non-ideal gas flow applications. *Energy* **2022**, *261*, 125143.
99. Passmann, M.; aus der Wiesche, S.; Joos, F. A one-dimensional analytical calculation method for obtaining normal shock losses in supersonic real gas flows. In *Journal of Physics: Conference Series*; IOP Publishing: Bristol, UK, 2017; Volume 821, p.012004. https://doi.org/10.1088/1742-6596/821/1/012004.
100. Span, R.; Wagner, W. Equations of state for technical applications. I. Simultaneously optimized functional forms for nonpolar and polar fuids. *Int. J. Thermophys*. **2003**, *24*, 1–39.
101. Colonna, P.; Nannan; NR; Guardone, A.; Lemmon, E.W. Multiparameter equations of state for selected siloxanes. *Fluid Phase Equilibria* **2006**, *244*, 193–211.
102. Colonna, P.; Nannan, N.R.; Guardone, A. Multiparameter equations of state for siloxanes[(CH3)3-Si-O1/2]2-[O-Si-(CH3)2]i=1,...,3, and [O-Si-(CH3)2]6. *Fluid Phase Equilibria* **2008**, *263*, 115–130.
103. Thol, M.; Dubberke, F.H.; Rutkai, G.; Windmann, T.; Köster, A.; Span, R.; Vrabec, J. Fundamental equation of state correlation for hexamethyldisiloxane based on experimental and molecular simulation data. *Fluid Phase Equilibria* **2016**, *418*, 133–151.
104. Thol, M.; Dubberke, F.H.; Baumhögger, E.; Vrabec, J.; Span, R. Speed of sound measurements and fundamental equations of state for octamethyltrisiloxane and decamethyltetrasiloxane. *J. Chem. Eng. Data* **2017**, *62*, 2633–2648.
105. Gori, G.; Molesini, P.; Persico, G.; Guardone, A. Non-Ideal Compressible-Fluid Dynamics of Fast-Response Pressure Probes for Unsteady Flow Measurements in Turbomachinery. In *Journal of Physics: Conference Series*; IOP Publishing: Bristol, UK, 2017; Volume 821, p. 012005.

106. Cozzi, F.; Spinelli, A.; Gallarini, S.; Guardone, A. Optical Diagnostics for Non-Ideal Compressible Fluid Dynamics. *Rcoftac Bull.* **2020**, *124*, 67–72.
107. Head, A.J.; Novara, M.; Gallo, M.; Schrijer, F.; Colonna, P. Feasibility of Particle Image Velocimetry for Low-Speed Unconventional Vapor Flows. *Exp. Therm. Fluid Sci.* **2019**, *102*, 589–594.
108. Settles, G.S. *Schlieren and Shadowgraph Techniques: Visualizing Phenomena in Transparent Media*; Springer Berlin/Heidelberg, Germany, 2001.
109. Merzkirch, W. *Flow Visualization*; Academic Press: Cambridge, MA, USA, 1987.
110. Conti, C.C.; Spinelli, A.; Cammi, G.; Zocca, M.; Cozzi, F.; Guardone, A. Schlieren visualizations of non-ideal compressible fluid flows. In *13th International Conference on Heat Transfer, Fluid Mechanics and Thermodynamics (HEFAT 2017)*, EDAS: Messina, Italy, 2017; pp. 513–518.
111. Cammi, G. Measurements Techniques for Non-Ideal Compressible Fluid Flows: Applications to Organic Fluids. Ph.D. Thesis, Politecnico di Milano, CREA Lab, Milan, Italy, 2019.
112. Zocca, M.; Guardone, A.; Cammi, G.; Cozzi, F.; Spinelli, A. Experimental observation of oblique shock waves in steady non-ideal flows. *Exp. Fluids* **2019**, *60*, 101.
113. Cozzi, F.; Göttlich, E.; Angelucci, L.; Dossena, V.; Guardone, A. Development of a background oriented schlieren technique with telecentric lenses for supersonic flow. In *Journal of Physics: Conference Series*; IOP Publishing: Bristol, UK, 2017; Volume 778, p. 012006.
114. Richard, H.; Raffel, M. Principle and applications of the background oriented schlieren (BOS) method. *Meas. Sci. Technol.* **2001**, *12*, 1576–1585.
115. Klinge, F.; Kirmse, T.; Kompenhans, J. Application of Quantitative Background Oriented Schlieren (BOS): Investigation of a Wing Tip Vortex in a Transonic Wind Tunnel. *Proc. PSFVIP4* **2003**, *4097*, 3–5.
116. Goldhahn, E.; Seume, J. The background oriented schlieren technique: Sensitivity, accuracy, resolution and application to a three-dimensional density field. *Exp. Fluids* **2007**, *43*, 241–249.
117. Venkatakrishnan, L.; Meier, G.E. Density measurements using the Background Oriented Schlieren technique. *Exp. Fluids* **2004**, *37*, 237–247.
118. Raffel, M. Background-oriented schlieren (BOS) techniques. *Exp. Fluids* **2015**, *56*, 1–17.
119. Clem, M.M.; Zaman, K.B.M.Q.; Fagan, A.F.; Glenn, N. 2012, Background Oriented Schlieren Applied to Study Shock Spacing in a Screeching Circular Jet. In Proceedings of the 50th AIAA Aerospace Sciences Meeting including the New Horizons Forum and Aerospace Exposition, Nashville, TN, USA, 9–12 January 2012; pp. 1–12.
120. Kindler, K.; Goldhahn, E.; Leopold, F.; Raffel, M. Recent developments in background oriented Schlieren methods for rotor blade tip vortex measurements. *Exp. Fluids* **2007**, *43*, 233–240.
121. Sundermeier, S.; Matar, C.; aus der Wiesche, S.; Cinnella, P.; Hake, L.; Gloerfelt, X. Experimental and numerical study of transonic flow of an organic vapor past a circular cylinder. In Proceedings of the 4th International Seminar on Non-Ideal Compressible Fluid Dynamics (NICFD2022), City University, London, UK, 3–4 November 2022, 2022.
122. Passmann, M.; aus der Wiesche, S.; Joos, F. Focusing Schlieren Visualization of Transonic Turbine Tip-Leakage Flows. *Int. J. Turbomach. Propuls. Power* **2020**, *5*, 1.
123. Schardin, H. Die Schlierenverfahren und ihre Anwendungen. In *Ergebnisse der Exakten Naturwissenschaften*, Springer: Berlin, Germany, 1942; pp. 303–439.
124. Weinstein, L. Large-Field High-Brightness Focusing Schlieren System. *AIAA J.* **1993**, *31*, 1250–1255.
125. Albrecht, H.-E.; Damaschke, N.; Borys, M.; Tropea, C. *Laser Doppler and Phase Doppler Measurement Techniques*; Springer: Berlin, Germany, 2013.
126. Gallarini, S.; Cozzi, F.; Spinelli, A.; Guardone, A. Direct velocity measurements in high-temperature non-ideal vapor flows. *Exp. Fluids* **2021**, *62*, 199.
127. Gallarini, S.; Spinelli, A.; Cozzi, F.; Guardone, A. Design and commissioning of a laser doppler velocimetry seeding system for non-ideal fluid flows. In Proceedings of the 12th International Conference on Heat Transfer, Fluid Mechanics and Thermodynamics, HEFAT, Costa de Sol, Spain, 11–13 July 2016.
128. Westerweel, J.; Elsinga, G.E.; Adrian, R.J. Particle image velocimetery for complex and turbulent flow. *Annu. Rev. Fluid Mech.* 2013, 45,409-436.
129. Raffel, M.; Willert, C.E.; Wereley, S.T.; Kompenhans, J. *Particle Image Velocimetry: A Practical Guide*; Springer: Berlin, Germany, 2007.
130. Ueno, W.; Tsuru, S.; Kinoue, Y.; Shiomo, N.; Setoguchi, T. PIV measurement of carbon dioxide gas-liquid two-phase nozzle flow. In Proceedings of the ASME-JSME-KSME Joints Fluids Engineering Conference, Seoul, Republic of Korea, 26–31 July 2015; AJKFluids2015-20169.
131. Valori, V. Rayleigh-Benard Convection of A Supercritical Fluid: (PIV) and Heat Transfer Study. Ph.D. Thesis, Delft University of Technology, Delft, The Netherlands, 2017.
132. Perry, A. *Hot-Wire-Anemometry*; Clarendon Press: Oxford, UK, 1982.
133. Fingerson, L.; Freymuth, P. Thermal Anemometers. In *Fluid Mechanics Measurements*; Goldstein, R., Ed.; Hemisphere: Washington, DC, USA, 1983.
134. Lomas, C. *Fundamentals of Hot Wire Anemometry*; Cambridge University Press: Cambridge, UK, 1986.
135. Bruun, H.H. *Hot-Wire Anemometry: Principles and Signal Analysis*; Oxford University Press: Oxford, UK, 1995.

136. Comte-Bellot, G. Hot-Wire Anemometry. *Annu. Rev. Fluid Mech.* **1976**, *8*, 209–231.
137. Kovasznay, L.S.G. The Hot-Wire Anemometer in Supersonic Flows. *J. Aeronaut. Sci.* **1950**, *17*, 565–584.
138. Spangenberg, W.G. *Heat Loss Characteristics of Hot-Wire Anemometers at Various Densities in Transonic and Supersonic Flow*; NACA Tech. Note No. 3381; National Advisory Committee for Aeronautics: Washington, DC, USA, 1955.
139. Morkovin, M.W. Fluctuations and Hot-Wire Anemometry in Compressible Flows, AGARDograph No. 24, NATO, Paris,1956.
140. Horstman, C.C.; Rose, W.C. Hot-Wire Anemometry in Transonic Flow. *AIAA J.* **1977**, *15*, 395–401.
141. Rose, W.C.; McDaid, E.P. Turbulence Measurement in Transonic Flow. *AIAA J.* **1977**, *15*, 1368–1370.
142. Stainback, P.C.; Johnson, C.B.; Basnett, C.B. Preliminary Measurements of Velocity, Density and Total Temperature Fluctuations in Compressible Subsonic Flow. In Proceedings of the AIAA 21st Aerospace Sciences Meeting, Reno, NV, USA, 10–13 January 1983; AIAA-83-0384.
143. Stainback, P.C. Some Influences of Approximate Values for Velocity, Density and Total Temperature Sensitivities on Hot Wire Anemometer Results. In Proceedings of the AIAA 24th Aerospace Sciences Meeting, Reno, NV, USA, 6–9 January 1986; AIAA-86-0506.
144. Stainback, P.C.; Nagabushana, K.A. Review: Hot-Wire Anemometry in Transonic and Subsonic Slip Flows. *ASME Fluids Eng.* **1997**, *119*, 14–18.
145. Motallebi, F. A Review of the Hot-Wire Technique in 2-D Compressible Flows. *Prog. Aerospace Sci.* **1994**, *30*, 267–294.
146. Johnston, R.; Fleeter, S. Compressible flow hot-wire calibration. *Exp. Fluids* **1997**, *22*, 444–446.
147. de Souza, F.; Tavoularis, S. Hot-Wire Response in High-Subsonic Flow. In Proceedings of the AIAA 37th Aerospace Sciences Meeting and Exhibit, Reno, NV, USA, 11–14 January 1999, AIAA-99-0310.
148. Cukurel, B.; Acarer, S.; Arts, T. A novel perspective to high-speed cross-hot-wire calibration methodology. *Exp. Fluids* **2012**, *53*, 1073–1085.
149. Reinker, F.; aus der Wiesche, S. Application of Hot-Wire Anemometry in the High Subsonic Organic Vapor Flow Regime. In *NICFD 2020, ERCOFTAC Series 28*; Pini, M., de Servi, C., Spinelli, A., di Mare, F., Guardone, A., Eds.; Springer International Publishing: Cham, Switzerland, 2021; pp. 135–143.
150. Hake, L.; Sundermeier, S.; Cakievski, L.; Bäumer, J.; aus der Wiesche, S.; Matar, C.; Cinnella, P.; Gloerfelt, X. Hot-Wire Anemometry in High Subsonic Organic Vapor Flows. In Proceedings of the ASME Turbo Expo 2022, Rotterdam, The Netherlands, 13–17 June 2022; GT2022-81686.
151. Hake, L.; aus der Wiesche, S.; Sundermeier, S.; Bienner, A.; Gloerfelt, X.; Cinnella, P. Grid-generated decaying turbulence in an organic vapor flow. In Proceedings of the 4th International Seminar on Non-Ideal Compressible Fluid Dynamics (NICFD2022), City University, London, UK, 3–4 November 2022.
152. Jones, G.S. Wind Tunnel Requirements for Hot-Wire Calibration. In Proceedings of the AIAA 18th Aerospace Ground Testing Meeting, Colorado Springs, CO, USA, 20–23 June 1994; AIAA-94-2534.
153. Yavuzkurt, S. A Guide to Uncertainty Analysis of Hot-Wire Data. *ASME J. Fluids Eng.* **1984**, *106*, 181–186.
154. Smolyakov, A.V.; Tkachenko, V.M. *The Measurement of Turbulent Fluctuations*; Springer: Berlin, Germany, 1983.
155. Wyngaard, J.C. Measurement of small-scale turbulence structure with hot wires. *J. Sci. Instrum.* **1968**, *1*, 1105–1108.
156. Hake, L.; Sundermeier, S.; aus der Wiesche, S.; Bienner, A.; Gloerfelt, X.; Matar, C.; Cinnella, P. CFD-supported data reduction of hot-wire anemometry signals for compressible organic vapor flows. In Proceedings of the XXVI Biennial Symposium on Measuring Techniques in Turbomachinery, Pisa, Italy, 28–30 September 2022.
157. Weiss, J.; Chokani, N.; Comte-Bellot, G. Constant-Temperature and Constant-Voltage Anemometer Use in a Mach 2.5 Flow. *AIAA J.* **2005**, *43*, 1140–1143.
158. Roediger, T.; Jenkins, S.; Knauss, H.; Wolfersdorf, J.; Gaisbauer, U.; Kraemer, E. Time-Resolved Heat Transfer Measurements on the Tip Wall of a Ribbed Channel Using a Novel Heat Flux Sensor—Part I: Sensor and Benchmarks. *ASME J. Turbomach.* **2008**, *130*, 011018.
159. Sieverding, C.; Manna, M. A Review on Turbine Trailing Edge Flow. *Int. J. Turbomach. Propuls. Power* **2020**, *5*, 10.
160. Sieverding, C.H.; Heinemann, H. The Influence of Boundary Layer State on Vortex Shedding from Flat Plates and Turbine Cascades. *ASME J. Turbomach.* **1990**, *112*, 181–187.